Chemical Science

ROYAL SOCIETY OF CHEMISTRY

EDGE ARTICLE

View Article Online
View Journal | View Issue

Cite this: *Chem. Sci.*, 2026, **17**, 6017

All publication charges for this article have been paid for by the Royal Society of Chemistry

Received 4th November 2025
Accepted 20th January 2026

DOI: 10.1039/d5sc08559d

rsc.li/chemical-science

Remote α- and β-C(sp^3)–H alkenylation of amines *via* visible-light supported paired electrolysis

Siddharth K. Dave and Sebastian Stecko *

A general method for photoelectrochemical site-selective α- and β-C(sp^3)–H alkenylation of amines with vinyl bromides has been developed. Regioselective activation of inert C–H bonds is achieved by intramolecular hydrogen atom abstraction (HAT) by an oxidatively generated aryl radical. Depending on the HAT directing group attached to the amines' N-atom, either 1,5- or 1,6-H-atom transposition occurred, leading to regioisomeric carbon-centered radical species. C-radicals thus formed at the α/β-position of the amines' functionality undergo radical cross-coupling with Ni complex-activated vinyl bromide to provide the corresponding α- or β-functionalized amines. Good functional group tolerance, gram-scale experiments, post-functionalization and demonstration of preparation of key structural scaffolds of the selected naturally occurring compounds and drug candidates greatly highlight the potential applicability of the presented method. The mechanistic experiments demonstrated that the reported protocol consists of a photoelectrochemically induced thiyl radical anodic cycle and an electrochemically driven Ni-catalytic cathodic cycle. The first one is responsible for the generation of $CO_2^{\bullet-}$, a XAT reagent capable of activation of aryl halide to provide aryl radical species. Cathodic reduction of a Ni(I) intermediate to the Ni(0) complex allows closing the Ni-catalyzed cycle, enabling the execution of the cross-coupling stage leading to a C–H functionalized amine derivative. The developed conditions enable precise synchronization of anodic and cathodic catalytic cycles occurring in the presented variant of paired electrolysis, which has been a significant challenge until now.

Introduction

The allylic amine moiety is a ubiquitous structural motif found in numerous bioactive molecules and naturally occurring compounds like anticancer maclekarpine E,[1,2] antimicrobial zanthocapensine[2–4] or alkaloid caulophyllumine[5] (Fig. 1). Furthermore, allylamines are versatile intermediates and building blocks, with numerous applications in organic synthesis. For instance, alkenylated heterocyclic scaffolds often serve as a direct precursor for the total synthesis of numerous alkaloids (*e.g.*, galipeine,[6,7] cuspareine,[6] galipinine,[6] angustureine,[6] dysoxyline,[8,9] and methofoline[8,9]) or heterocyclic drugs (*e.g.*, almorexant,[10,11] iferanserin,[12] and encainide[13,14]) presented in Fig. 1.

Classic methods for allylamine synthesis rely on nucleophilic substitution by amines,[15,16] including Tsuji-Trost allylic amination,[15,17–19] vinylation of imines,[20,21] reductive amination of enals or enones,[22] or sigmatropic rearrangement reactions.[23–25] Although these are well-established protocols in synthetic organic chemistry, they also exhibit several drawbacks, like the use of stoichiometric amounts of organometallic reagents, insufficient levels of stereocontrol, or the formation of numerous side products. So far, the Pd- or Ir-catalyzed Tsuji-Trost allylic amination reaction seems to be the most efficient strategy to deliver linear or branched allylamines (depending on the metal catalyst used) by reacting amines with various allylic electrophiles.[15,17–19] Nevertheless, even this strategy still encounters challenges and drawbacks, particularly in the preparation of α-alkenylated saturated aza-heterocycles.

From the synthetic perspective, direct regio- and stereoselective α-C(sp^3)–H alkenylation is regarded as the most attractive strategy for synthesizing the mentioned types of allylamines since it starts with inexpensive, readily available cyclic amines (Scheme 1a).[26–28] The classic approaches involve deprotonation by organolithium reagents, followed by transition metal-mediated cross-coupling with vinyl halide reagents (Scheme 1a). An alternative approach is direct C–H bond activation by transition metal complexes followed by coupling with a vinyl reagent (Scheme 1a).[28] Alkynes, in addition to vinyl halides, can serve as effective alkenylating agents (Scheme 1a).[28–30] Nevertheless, the use of a strong base significantly limits the substrate scope in the first case, whereas the requirement of expensive metal complexes and harsh reaction conditions significantly limits the efficiency of the second process. Moreover, both cases require specific directing groups to achieve regioselective activation of the α-C–H bond, and these groups must be removed in further steps. A less explored

Institute of Organic Chemistry, Polish Academy of Sciences, Marcina Kasprzaka Street 44/52, 01-224 Warsaw, Poland. E-mail: sebastian.stecko@icho.edu.pl

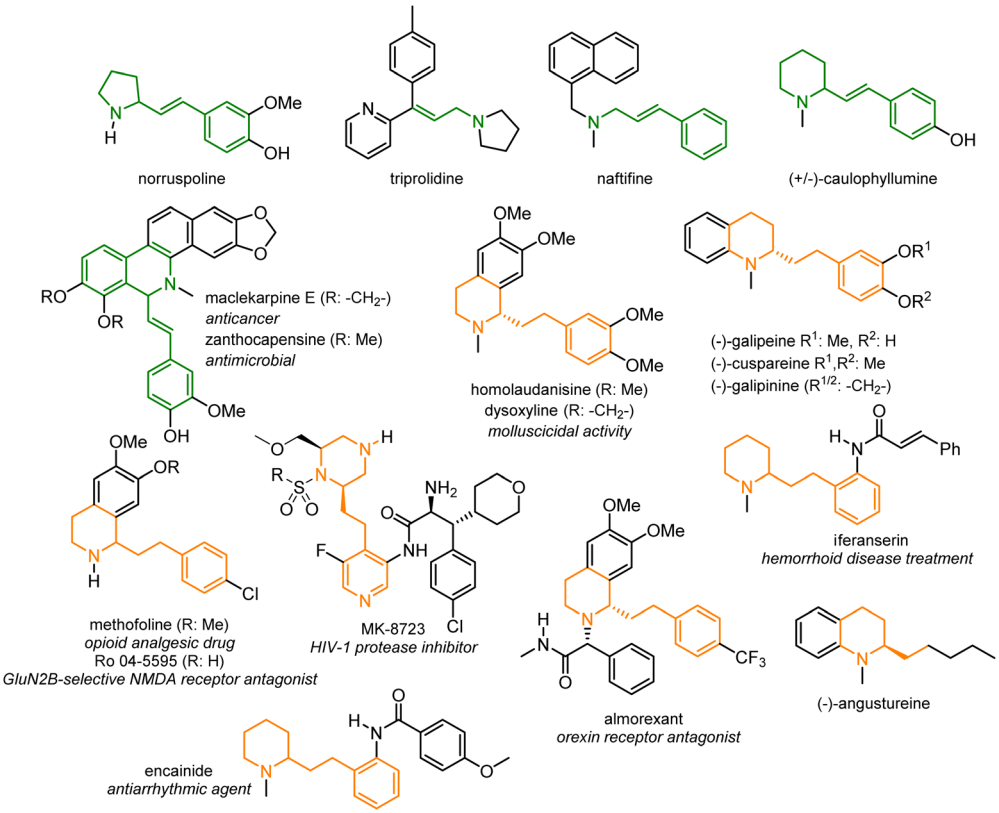

Fig. 1 Representative bioactive compounds containing an allylic amine moiety (in green) and bioactive molecules obtained from the corresponding allylamine precursors (in yellow).

approach for the synthesis of complex allylamines relies on functionalization, for instance arylation or alkylation, of allylamine derivatives, *e.g.*, allylamine vinyl bromides, through their reactions with arylating agents (*e.g.*, arylboronic acids)[31–33] or alkylating reagents,[18a,33] including alkyl radical precursors (*e.g.*, alkyl halides, carboxylic acids, *etc.*) under photoredox[34,35] (Scheme 1b).

Intensive developments in modern organic photochemistry brought new concepts in the synthesis of allylamines, particularly methods involving the generation and alkenylation of α-aminoalkyl radical species (Scheme 1a). In their pioneering studies, MacMillan and co-workers[36,37] demonstrated conditions for Ir-catalysed photoredox vinylation of tertiary *N*-aryl amines with vinyl sulfones. The key intermediates, α-aminoalkyl radical species, were generated either from amines *via* an SET/deprotonation sequence or through the decarboxylation of amino acids, mediated by a photoexcited Ir complex acting as a strong oxidant. A few years later, Xie and co-workers[38] employed this approach for the total synthesis of maclekarpine E (Fig. 1) and its analogues.

The intramolecular 1,5-hydrogen atom transfer (1,5-HAT) strategy is another method for the generation of α-aminoalkyl radical species (*e.g.*, **INT-B**).[39–45] It has recently gained a lot of attention as a powerful tool for selective C–H bond functionalisation, introducing various functional groups and delivering complex molecules. This method often involves using a substrate with a pre-installed functional group that operates as a source of reactive radical intermediates (*e.g.*, **INT-A**), serves as a directing group to control the 1,5-HAT process, and acts as a protective group. In 2022, Gevorgyan and his team[46] reported a simple and effective method for adding a boron group to the α-C–H bond of 2-iodobenzoyl-protected secondary amines, resulting in the formation of α-amino boronic acids (Scheme 1c(i)). The key step of this process was single-electron transfer (SET) or halogen-atom transfer (XAT) cleavage of the C(sp^2)–I bond to generate an aryl radical (*e.g.*, **INT-A**). This species is capable of subsequent 1,5-hydrogen atom abstraction from the α-C position of secondary amine. The trapping agent, such as B_2cat_2, then intercepts the resulting alkyl radical (*e.g.*, **INT-B**) to produce a functionalised product. Soon after, Zhang's group[47] demonstrated a visible-light-induced asymmetric C(sp^3)–H Cu-catalysed alkynylation of cyclic tertiary amines initiated by the 1,5-HAT process. After this research, both the Wang group[48] and the Saget group (Scheme 1c(ii))[49] and others developed similar methods, using aryl radicals to start the 1,5-HAT process for the α-C–H functionalisation of secondary amines with Michael acceptors, while Sureshkumar and others reported the conditions for photoredox α-C–H alkylation using [1.1.1]-propellane.[50] Several reports also described the α-C–H arylation method through cross-coupling of α-aminoalkyl radicals with heteroarenes. The pool of potent trapping agents that can be used for such radical remote C–H functionalisation includes phosphites (α-C–H phosphonation, Scheme 1c(iii)),[51] aldehydes (α-C–H acylation),[52] silyl reagents (α-C–H silylation, Scheme

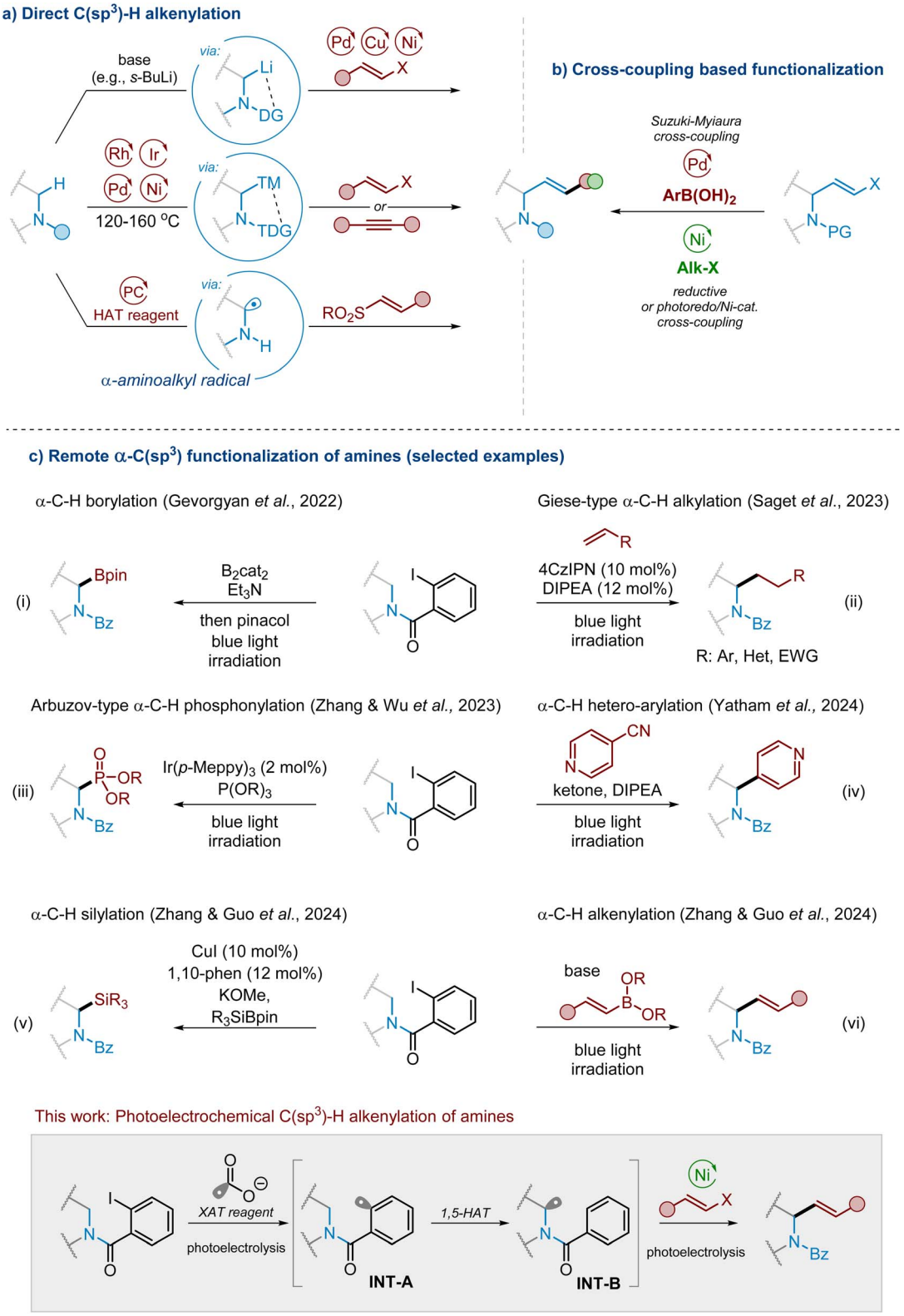

Scheme 1 Background and concept design: (a) traditional direct α-C(sp^3)–H alkenylation of amines; (b) divergent functionalization of allylamine vinyl bromides; (c) remote α-C(sp^3)–H functionalization of amines.

1c(v)),[53] imines (α-C–H aminoalkylation) and azides (α-C–H azidation).[54] Surprisingly, an analogous concept for α-C–H alkenylation of cyclic amines is almost unknown so far, with only one report on the related aryl radical-mediated α-C(sp^3)–H alkenylation of secondary amines by Guo, Zhang, and their co-workers (Scheme 1c(vi)).[55] They employed the ate complexes of

vinylboronic acid esters and alkoxides as alkenylation agents. This ate complex interacted with the secondary amine substrate to deliver an EDA complex, which underwent photoexcitation to generate an aryl radical from the 2-iodobenzoyl group attached to the amine nitrogen atom. The subsequent 1,5-HAT process produced the desired 2-alkenylated products in excellent yield by intercepting the alkyl radical with the activated alkenylboronic acid. Although this method is quite elegant, some drawbacks related to the employed reaction conditions still leave a space for further improvements and advancements in terms of substrate diversity, cost-effectiveness, and reaction selectivity.

We questioned if vinyl halides, instead of vinyl boronic acid derivatives, could serve as suitable reagents for the aforementioned C–H alkenylation of secondary amines through the 1,5-HAT/cross-coupling sequence facilitated by aryl radicals. Based on the previous reports, we decided to use the 2-halogenbenzoyl group to produce aryl radicals, which should deliver the α-aminoalkyl radical after the 1,5-HAT process; this radical is designed to react with the Ni(II)-alkene complex generated from the vinyl halide and Ni(0). Our primary objective was to establish conditions suitable for the activation of both reaction partners. This phase appeared to be the most challenging, as the Ni(0) complex may activate both the vinyl halide and the aryl halogen moiety of the HAT-directing group. Consequently, our primary task was to develop conditions for the effective activation of the directing group and the ensuing cross-coupling process with activated vinyl halide. The next objective was to synchronise all three steps: aryl radical generation, 1,5-HAT and cross-coupling within the specified sequence. This issue was critical because failing to meet the correct conditions may predominantly lead to undesired homocoupling and dehalogenation products from the starting materials, resulting in a complex reaction mixture.

Results and discussion

Development of reaction conditions

With our hypothesis in mind, we started exploring the feasibility of our proposed alkenylation reaction. We chose 2-iodobenzoyl-protected morpholine **1a** and vinyl bromide **2a** as model substrates. The reaction between them was performed in the presence of Ni(glyme)Br_2 (10 mol%) and 4,4′-di-*t*-butyl-2,2′-bipyridine (dtbbpy) (12 mol%) which formed the corresponding Ni-complex for the final cross-coupling step.[34,56]

Initially, we examined diverse photochemical conditions for the reductive generation of aryl radical **INT-A**. In preliminary studies, we adapted the conditions for the generation of aryl radicals described by Doyle[57,58] and others[59] and the alkenylation of **1a** with **2a** was conducted using an Ir complex, as a photocatalyst, K_3PO_4 as a base and TBABr as a source of Br radicals acting as an XAT reagent. The model reaction was performed in MeCN under blue light irradiation (450–460 nm) (Scheme 2, ent. 1a). While complete conversion of **1a** took place, only traces of desired product **3aa** were detected (as determined by GC analysis), alongside the deiodination product **4a** and the homocoupling product of vinyl bromide **2a**. Further modifications to these reaction conditions, including variations in the nickel source (*e.g.*, Ni(glyme)Cl_2, Ni(cod)$_2$, NiI_2, *etc.*), base (K_2CO_3, K_2HPO_4, KH_2PO_4, Na_2CO_3, *etc.*), or solvent(s) (*e.g.*, DMF, MeCN, *etc.*), failed to enhance the process, with product **4a** remaining predominant. Next, we turned our attention to the Leonori studies[60] revealing trialkylamines as potent XAT reagents for the generation of aryl radicals from the corresponding aryl halides.[49,66] Adapting the Leonori report,[60] the model alkenylation reaction was conducted with 4-CzIPN as a photocatalyst and Hünig's base as an XAT reagent.[61] Unluckily, the conversion of **1a** was quite low (45%) and again merely traces of the expected product were detected (Scheme 2, ent. 2a). Furthermore, any further modifications to the reaction conditions, such as altering the photocatalyst (*e.g.*, 4-DPAIPN,[67,68] 3-DPA(F)IPN, 4-Cl-CzIPN, and [Ir(dFppy)$_2$(dtbbpy)]PF_6) or changing the employed trialkylamine reagent (*e.g.*, Et_3N, *n*-Bu_3N, *etc.*), were unsatisfactory. The same result was obtained when the HAT reagent, aryl radical, was formed *via* a C(sp^2)–I bond cleavage by a silyl radical, as reported by Yang and Guo.[69,70] In this case, tris(trimethylsilyl)silane (TTMS) acted as a source of an XAT reagent produced photochemically with or without a photocatalyst (Scheme 2, ent. 3a and 3b). Under both conditions, the competitive reductive dehalogenation of the heterocyclic substrate occurred more rapidly than the expected Ni-catalyzed cross-coupling process. We have also examined the protocol outlined by Sureshkumar,[50] wherein 2-iodobenzoyl-protected amines, *e.g.* **1a**, with the carbonate anion form an electron donor–acceptor complex (EDA complex), which upon irradiation (440 nm) should undergo photoexcitation and generate the aryl radical (*via* homolysis of the C–I bond) for the subsequent 1,5-HAT step.

Disappointingly, upon implementing the specified conditions (Scheme 2, ent. 4a), we neither observed the generation of product **3aa** nor even product **4a** and recovered entire starting material **1a**. Our spectroscopic studies confirmed that compound **1a** forms the EDA complex with carbonate ions postulated by authors, as indicated by the bathochromic shift of the absorption band for **1a** from *ca.* 290 nm to 332 nm (see SI, Fig. SI-8). Nonetheless, this maximum is evidently beyond the spectrum of the light source employed by the authors (Kessil™ LED lamp 440 nm),[71] hence precluding any potential for photoexcitation of the specified complex!

In light of the above observations and evidence, we decided to repeat this experiment using higher-energy light sources. Upon irradiating the reaction mixture with light at a wavelength of 395 nm (Scheme 2, ent. 4b), we observed complete conversion of the substrate **1a**, but the yields of the desired product **3aa** were below 10%. Similarly, when irradiating with light at a wavelength of 365 nm (Scheme 2, ent. 4c), substrate **1a** underwent complete conversion; however only traces of **3aa** were noticed by a GC analysis.

The lack of success of a photochemical approach forced us to investigate the generation of the aryl radical for the 1,5-HAT process under electrochemical conditions *via* either the direct or electromediator-aided pathway (Scheme 2, ent. 6a–d).[72–74] Following the protocol for an electroreduction of aryl iodides reported by Wang,[63] we electrolyzed the model reaction mixture in an electrochemical cell equipped with a Ni-anode and

1a **2a** **3aa** **4a**

Ent.	Conditions	Conv. of **1a**	Yield of **3aa**	Yield of **4a**	Ref.
1a.	$[Ir(ppy)_2(dtbbpy)]PF_6$ (1 mol%), K_3PO_4 (3 eq), MeCN, 26 °C, TBABr (5 eq), blue light irradiation (450-460 nm)	>99%	traces (GC)	87% (isol.)	57, 58
1b.	$[Ir(dF(CF_3)ppy)_2(dtbbpy)]PF_6$ (1 mol%), Hantzch's ester (3 eq), MeCN, 26 °C, blue light irradiation (450-460 nm)	>99%	traces (GC)	90% (isol.)	59
2a.	4-CzIPN (2 mol%), *i*-Pr_2NEt (3 eq), DMSO, 26 °C, blue light irradiation (450-460 nm)	45%	traces (GC)	27% (isol.)	60
2b.	4-CzIPN (2 mol%), Et_3N (3 eq), DMSO, 26 °C, blue light irradiation (450-460 nm)	57%	traces (GC)	33% (isol.)	-
2c.	4-CzIPN (2 mol%), *n*-Bu_3N (3 eq), DMSO, 26 °C, blue light irradiation (425 nm)	61%	traces (GC)	41% (isol.)	-
3a.	TTMS (2 eq), DCE, 26 °C, blue light irradiation (450-460 nm)	>99%	traces (GC)	90% (isol.)	61
3b.	4-CzIPN (2 mol%), TTMS (2 eq), DCE, 26 °C, blue light irradiation (450-460 nm)	>99%	traces (GC)	89% (isol.)	-
4a.	Cs_2CO_3 (3 eq), DMSO, 26 °C, blue light irradiation (440 nm)	0%	0% (GC)	0% (GC)	50
4b.	Cs_2CO_3 (3 eq), DMSO, 26 °C, blue light irradiation (395 nm)	>99%	<10% (GC)	70% (isol.)	-
4c.	Cs_2CO_3 (3 eq), DMSO, 26 °C, blue light irradiation (365 nm)	>99%	traces (GC)	83% (isol.)	-
5	4-DPAIPN (2 mol%), mesna **5aa** (20 mol%), HCOOCs (3 eq), DMSO, blue light irradiation (440 nm)	>99%	~15% (NMR)	68% (isol.)	62
6a.	(+)Ni|Graphite(-), TBACl (1 eq), DMF, rt, 15 mA, 6 h	>99%	traces (GC)[b]	35% (isol.)	63
6b.	(+)Zn|Graphite(-), $TBABF_4$ (1 eq), DMSO/MeCN 9:1 v/v, 40 °C, 9 mA, 4 h	90%	traces (GC)[b]	62% (isol.)	64
6c.	(+)Graphite|SS(-), $TBABF_4$ (1 eq), phenantrene (1 eq). MeCN 12 mA, 4 h	92%	traces (GC)[b]	55% (isol.)	65
6d.	(+) RVC|Ni_{foam}(-), $TBABF_4$ (2 eq), HCOOCs (3 eq.), thiol **5ab** (30 mol%), DMSO, 28 °C, 3 mA, irradiation (395 nm), 12 h	91%	35% (GC)[c]	43% (isol.)	-

[a] determined by GC, [b] formation of homo- and cross-coupling products;[c] the E/Z ratio 81:19; DCE = dichloroethane; TTMS = $(TMS)_3SiH$; ppy = 2-phenylpyridine; dtbbpy = 4,4'-di-t-butyl-2,2'-bipyridine; SS = stainless steel, PMP = 4-methoxyphenyl.

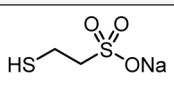

5aa

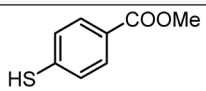

5ab

Scheme 2 Screening of initial conditions. PMP = 4-methoxyphenyl.

graphite cathode (Scheme 2, ent. 6a); however mostly we observed the formation of homo- and cross-coupling products. The further modification of reaction conditions, like the change of electrolyte and solvent, did not provide significant improvement. The change of the sacrificial anode material to Zn,[64] Al,[75] Mg[76] or steel[65] along with the use of an electromediator, *e.g.*, phenanthrene, provided 10–15% of the desired product along with homo-/cross-coupling side products. An important observation from these experiments was the high conversion of **1a**, although the formation of **3aa** and deiodination product **4a** was not noticed. Instead of this we observe the formation of a mixture of homo- and cross-coupling products of **1a** and **2a** indicating that the examined electrochemical conditions are capable of efficiently executing Ni-catalytic cycles, plausibly due to reduction of Ni(I) species to the key Ni(0) one.

Finally, we turned our attention to the reduction of aryl halides by a carbon dioxide radical anion ($CO_2^{\bullet-}$). This radical species is a valuable synthetic intermediate, thanks to extremely negative reduction potential ($E_{1/2(red)}$ $(CO_2/CO_2^{\bullet-}) = -2.2$ V *vs.* SCE)[77] and reactivity that makes it an efficient reductant and carboxylating agent.[78] Moreover, it can be easily generated from readily available formic acid salts by photoredox-HAT protocols in the presence of photocatalysts and additional hydrogen transfer reagents, commonly thiols.[78]

Initially, we employed the protocol for a photoinduced remote Giese-type C–H alkylation of amines in the presence of HCOOCs, reported by Yatham *et al.*[79] Thus, the mixture of model substrates **1a** and **2a** along with the Ni-complex and HCOOCs in DMSO was irradiated with purple light (390 nm). The starting material **1a** was consumed completely after 12 h to provide mostly product **4a** along with traces of **3aa** and small amounts of cross- or homo-coupling products. Based on the last observation, we conclude that these conditions were not suitable to execute the complete Ni-complex catalytic cycle.

Therefore, guided by seminal reports by Ju,[80] Wickens[68] and Jui[81] and our previous experience in the generation of the CO_2 anion radical,[62] we modified reaction conditions by introducing a photocatalyst (PC), like 4-CzIPN, and thiol **5aa** (mesna) to enhance the generation of the required XAT reagent through a thiyl radical-aided HAT from the formate anion (Scheme 2, ent. 5). Additionally, we expected that, generated under reaction conditions, the PC-derived radical anion will also serve as a reductant for Ni(I) species to deliver Ni(0) to close the cross-coupling catalytic cycle. Now, the activation of substrate **1a** proceeded efficiently, but product **4a** still dominated. The yield of **3aa** did not exceed 15%. The replacement of 4-CzIPN with 4-DPAIPN and the use of other thiols than mesna resulted in a slight improvement only. This confirmed our previous suspicions about the inefficient synchronicity of HAT and Ni-catalyzed cross-coupling steps; thus, we hypothesized that better synchronization of the reaction rates of individual processes should break the current impasse and significantly increase the efficiency of the process. Therefore, considering previous observations indicating that electrochemical conditions should enable the effective realization of the nickel catalytic cycle and the substrate **1a** activation strategy based on photoinduced-XAT, we decided to combine these strategies and investigate the possibility of alkenylation of compound **1a** with vinyl bromide **2a** under photoelectrochemical conditions.

In initial photoelectrochemical experiments, the mixture of vinyl bromide **2a** and morpholine derivative **1a**, containing HCOOCs, thiol **5ab** and Ni-complex ($Ni(glyme)Cl_2$ + dtbbpy) in DMSO, was irradiated (395 nm) and electrolyzed (3 mA) for 12 h. The initial electrochemical setup consisted of an undivided

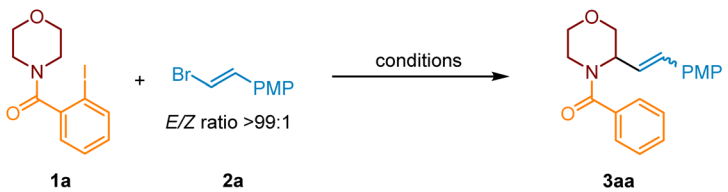

1a **2a** **3aa**

The modified parameter is marked in a color

Entry	Ni salt	ligand	formate salt	thiol	solvent	light	electrodes[a]	Conv. of **1a**[b]	Yield of **3aa**[b]	E/Z ratio
1.	$Ni(glyme)Cl_2$	dtbbpy	HCOOCs	**5aa**	DMSO	395 nm	(+) RVC | Ni_{foam} (-)	78%	6%	82 : 18
2.	$Ni(glyme)Br_2$	dtbbpy	HCOOCs	**5aa**	DMSO	395 nm	(+) RVC | Ni_{foam} (-)	89%	51%	96 : 04
3.	$Ni(glyme)Br_2$	PyBOX	HCOOCs	**5ab**	DMSO	395 nm	(+) RVC | Ni_{foam} (-)	>99%	67%	60 : 40
4.	$Ni(glyme)Br_2$	dtbbpy	HCOOK	**5ab**	DMSO	395 nm	(+) RVC | Ni_{foam} (-)	89%	51%	89 : 11
5.	$Ni(glyme)Br_2$	PyBOX	HCOOCs	**5aa**	DMSO	395 nm	(+) RVC | Ni_{foam} (-)	78%	6%	86 : 14
6.	$Ni(glyme)Br_2$	dtbbpy	HCOOCs	**5ba**	DMSO	395 nm	(+) RVC | Ni_{foam} (-)	>99%	51%	90 : 10
7.	$Ni(glyme)Br_2$	PyBOX	HCOOCs	**5ab**	MeCN	395 nm	(+) RVC | Ni_{foam} (-)	68%	9%	92 : 08
8.	$Ni(glyme)Br_2$	PyBOX	HCOOCs	**5ab**	DMF	395 nm	(+) RVC | Ni_{foam} (-)	63%	16%	93 : 07
9.	$Ni(glyme)Br_2$	PyBOX	HCOOCs	**5ab**	DMSO	400 nm	(+) RVC | Ni_{foam} (-)	>99%	38%	62 : 38
10.	$Ni(glyme)Br_2$	PyBOX	HCOOCs	**5ab**	DMSO	427 nm	(+) RVC | Ni_{foam} (-)	>99%	72%	65 : 35
11.	$Ni(glyme)Br_2$	PyBOX	HCOOCs	**5ab**	DMSO	440 nm	(+) RVC | Ni_{foam} (-)	>99%	56%	62 : 38
12.	$Ni(glyme)Br_2$	PyBOX	HCOOCs	**5ab**	DMSO	395 nm	(+) RVC | RVC (-)	>99%	57%	59 : 41
13.	$Ni(glyme)Br_2$	PyBOX	HCOOCs	**5ab**	DMSO	395 nm	(+) GRF | Ni_{foam} (-)	>99%	42%	83 : 17
14.	$Ni(glyme)Br_2$	PyBOX	HCOOCs	**5ab**	DMSO	395 nm	(+) GRF | GRF (-)	>99%	65%[c]	68 : 32
15.	$Ni(glyme)Br_2$	PyBOX	HCOOCs	**5ab**	DMSO	427 nm	(+) GRF | GRF (-)	>99%	87%[c]	72 : 28

[a] current 3mA; [b] determined by GC; [c] with alternating electrode polarity ever 10 min; RVC = reticulated vitreous carbon, GRF = graphite.

Optimized conditions for a model reaction

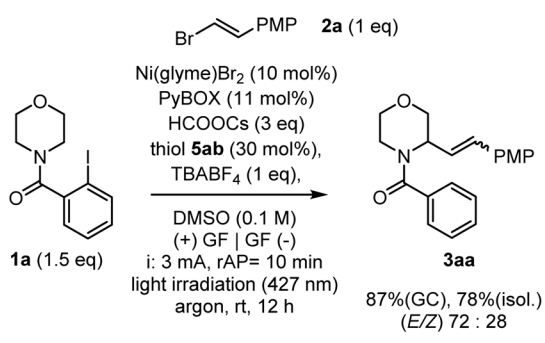

1a (1.5 eq) **3aa**

87%(GC), 78%(isol.)
(*E*/*Z*) 72 : 28

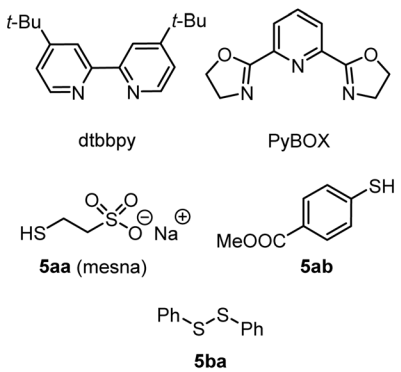

Scheme 3 Optimization studies on photoelectrochemical C–H alkenylation of amines (selected examples). PMP = 4-methoxyphenyl.

electrochemical cell equipped with RVC and $Ni_{(foam)}$ as an anode and a cathode, respectively. $TBABF_4$ was used as an electrolyte. Under these conditions, the expected product **3aa** was obtained in 35% yield (conversion of **1a** 91%) along with side product **4a** (Scheme 2, ent. 6d). This promising result encouraged us for further optimization of this process (Scheme 3).

We started the optimization of the photoelectrochemical protocol from examination of the influence of Ni salt on the products' yield. The replacement of Ni(glyme)Cl_2 with Ni(glyme)Br_2 allowed the product yield to be increased from 35% to 51% (Scheme 3, ent. 2). For other Ni salts, like NiI_2, $Ni(OTf)_2$ or $Ni(cod)_2$, the yields were much lower (see SI, Section 4.2.1.1). Next, we focused on the ligand choice. Initially 4,4′-di-*tert*-butyl-2,2′-bipyridine (dtbbpy) was used; however, further experiments demonstrated that the best results can be achieved when the Ni-complex with the PyBOX ligand was employed (Scheme 3, ent. 3

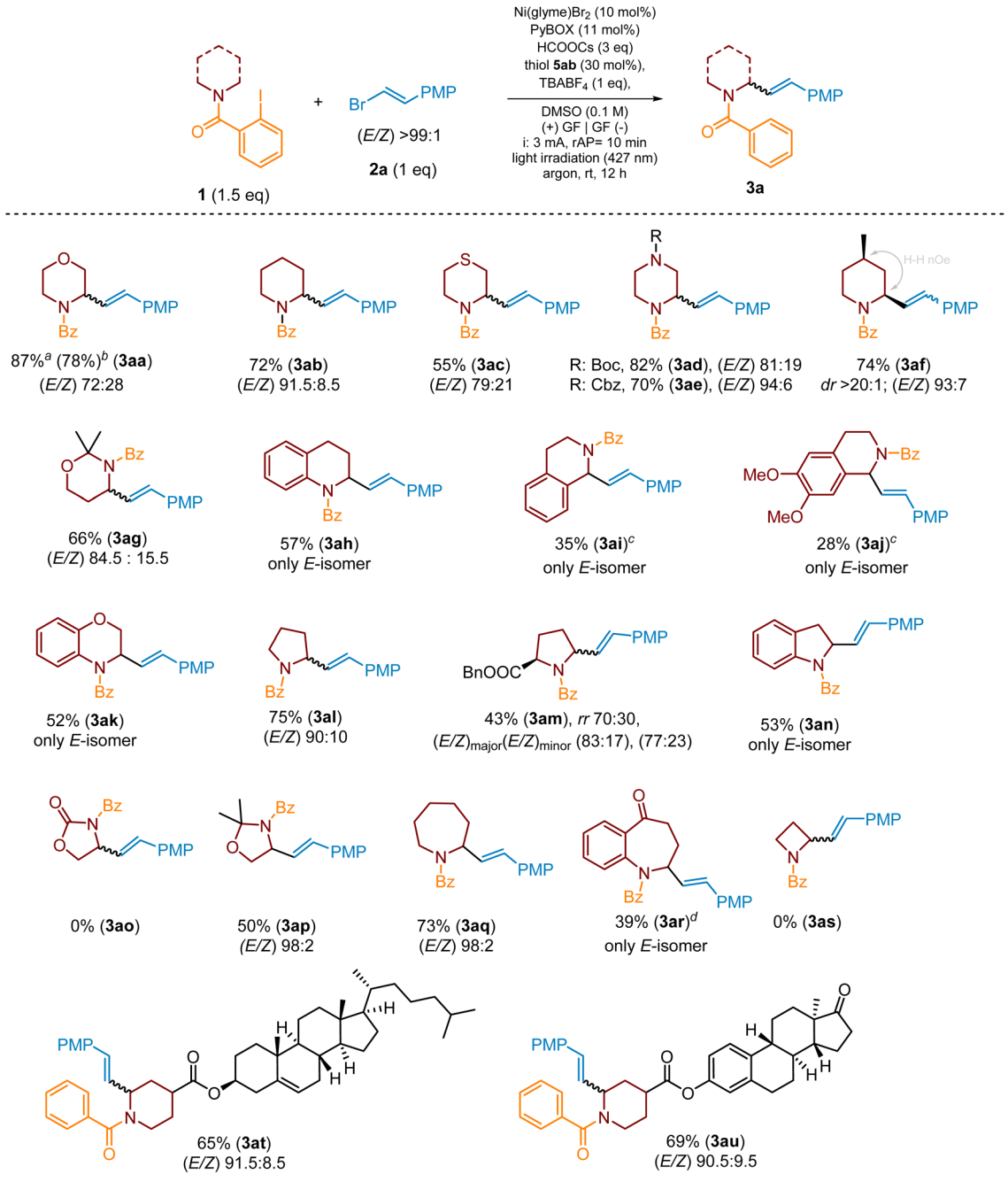

[a] yields assigned by GC with an internal standard, (*E*/*Z*) ratio assigned by ^{1}H NMR or GC; [b] isolated yield; [c] conv. 50% of benzamide after 12 h; [d] along with deiodinated starting material (ca. 20%). *rr* = regioisomers' ratio; PMP = 4-methoxyphenyl

Scheme 4 The scope of amines for remote α-C(sp^3)–H alkenylation of heterocycles **1**.

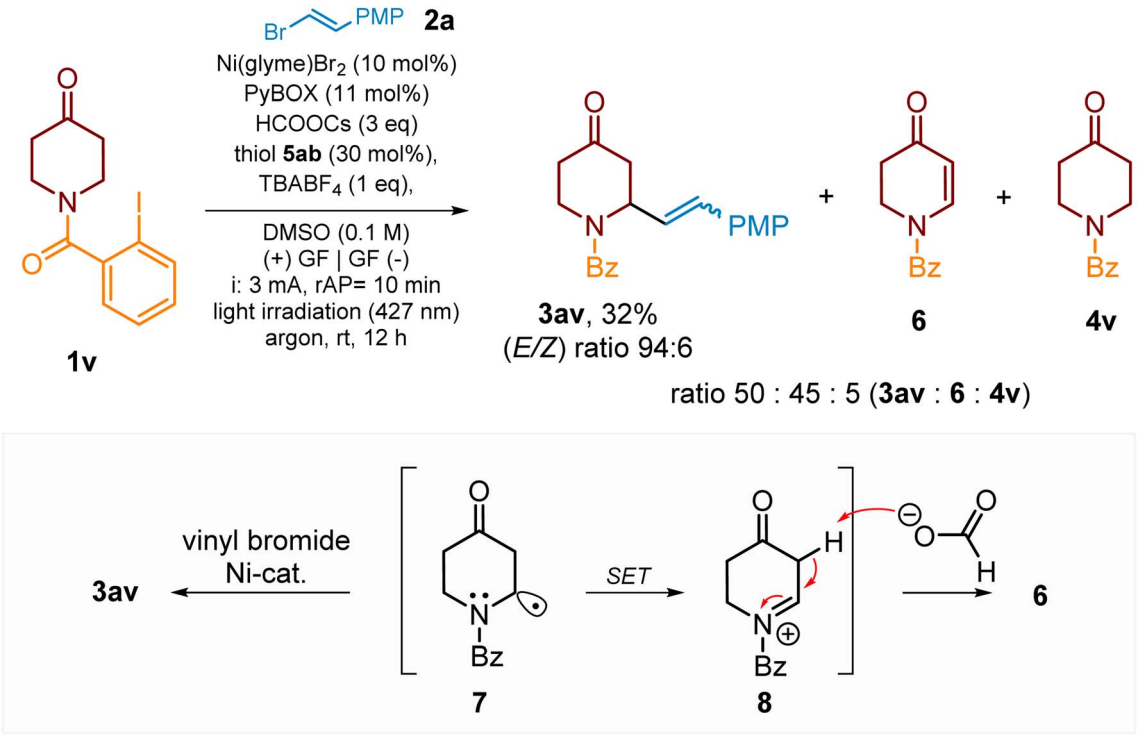

Scheme 5 The C–H alkenylation of piperidin-4-one derived benzamide **1v**. PMP = 4-methoxyphenyl.

and SI, Section 4.2.1.2). Initially, 10 mol% loading of Ni salt and 11 mol% of PyBOX ligand were employed; however, we found out that these amounts can be lowered to 5 mol% and 5.5 mol%, respectively, without significant change of SM's conversion and product's yield after the standard 12 hours. A further decrease in the amount of Ni salt to 3 mol% decreased conversion of **1a** from >99% to 67% and product yield to 53% after the standard 12 h (see SI, Section 4.2.2.2).

Among various formate salts, HCOOCs was the reagent of choice mostly due to its best solubility in DMSO compared to other formats (see SI, Section 4.2.1.4). The conversions of **1a** in the presence of K, Na or Li formate were in the range of 42–66%, and only traces of product **3aa** were detected. Interestingly, tetrabutylammonium formate (HCOOTBA) allowed for complete conversion of **1a** but the yield of **3aa** was less than 40%, indicating that it affected the cross-coupling step (see SI, Section 4.2.1.4).

Initially mesna (**5aa**) was used as a HAT reagent. However, an examination of other thiols (see SI, Section 4.2.1.3) revealed that methyl 4-mercaptobenzoate (**5ab**) provides complete conversion of **1a** and the highest yield of **3aa** (67%). Interestingly, its *ortho*-isomer delivered product **3aa** only in 37% (see SI, Section 4.2.1.3). In the case of the electron-rich aromatic thiols (*e.g.*, 4-mercaptoanisol) and aliphatic thiols (*e.g.*, CySH or methyl mercaptoacetate) the yields of the model product did not exceed 20%, despite over 90% conversion of starting material **1a** (see SI, Section 4.2.1.3).

As already mentioned, DMSO resulted in being the solvent of choice which assures proper solubility of all reagents, including $TBABF_4$ (1 equiv.) which served as an electrolyte of choice (see SI, Section 4.2.1.5). The optimal concentration was 0.1 M with respect to substrate **1a**. Higher dilution (0.05 M) caused a dramatic decrease in yield of **3aa** and an increase in the content of the reduced substrate (**4a**). In the case of other solvents, like MeCN or DMF, the conversion of **1a** was *ca.* 60% (after 12 h), but the product's yield was <15%, indicating that these solvents strongly affect the cross-coupling step (Scheme 3, ent. 7 and 8) (see SI, Section 4.2.1.6). Furthermore, the solvent mixtures, like DMSO/water or DMSO/MeCN, were examined to improve the yield of the reaction; however, all of these attempts were not successful (see SI, Section 4.2.1.6).

Finally, we focus on an optimization of photochemical and electrochemical conditions. Initial conditions, a constant current electrolysis (3 mA) in the presence of an RVC anode and a Ni foam cathode along with purple light irradiation (395 nm), provided the product **3aa** in 67% yield (Scheme 3, ent. 3). The use of light sources with longer wavelength light resulted in a significant decrease in the product's yield, except in the experiment when blue light with a wavelength of 427 nm was applied (ent. 3 and 9–11). In this case, the yield of the product increased up to 72% (ent. 10). The replacement of the RVC electrode with a graphite one resulted in a lower yield (*ca.* 42%, ent. 13). However, when two graphite electrodes were used instead of RVC and Ni(foam) ones, the model product was obtained in 65% (irradiation at 395 nm) (ent. 14) and 87% (irradiation at 427 nm) (ent. 15) yields. Additionally, we have also checked the influence of the applied current by varying it from 1 to 4 mA (see SI, Section 4.2.3.2). A current of 3 mA was optimal.

During optimization studies, we found out that the efficiency of the cross-coupling process decreased during the experiments due to "poisoning" of the anode by deposition of solid by-

products at the electrode surface. To avoid this, we set up a power supply to periodically change the polarization of the electrodes. We examined different polarization changing times, 5, 10, and 15 min, and the 10 min intervals were optimal (3 mA for 10 min and then −3 mA for 10 min). The alternating current electrolysis[82] with time intervals less than 60 s was ineffective, and the target product was obtained in yields below 65%. Therefore, irradiation with purple light (395 nm) and electrolysis with polarization change of two graphite electrodes every 10 min resulted in an increase in the product yield up to 65% (Scheme 3, ent. 14). Finally, the change in the light wavelength from 395 nm to 427 nm allowed for further improvement of the process and yielded the product **3aa** in 87%.

Finally, among 2-halobenzamides, the iodo-derivative, *e.g.*, **1a**, demonstrated superior reactivity and efficiency of the alkenylation process (see SI, Section 4.3.1). In the context of vinyl halides, vinyl bromide **2a** emerged as the superior cross-coupling partner, owing to its exceptional combination of stability and reactivity (see SI, Section 4.3.2).

The final optimization studies were devoted to elaborate the optimal amounts of the required reagents. Thus, the reaction of **1a** and **2a** in a ratio of 1 : 1.5, in the presence of 1 equiv. of $TBABF_4$, 3 equiv. of HCOOCs, 30 mol% of thiol **5ab**, 10 mol% of $Ni(glyme)Br_2$, and 11 mol% of PyBox ligand in DMSO (0.1 M), yielded product **3aa** in 87% (GC) as a mixture of *E*/*Z* isomers in a ratio of 72 : 28 (Scheme 3). Aqueous work-up of the post-reaction mixture followed by flash column chromatography delivered **3aa** in 78% isolated yield.

Substrates' scope

With optimal conditions in hand, we next explored the scope of the aryl radical-triggered remote C(sp^3)–H alkenylation protocol

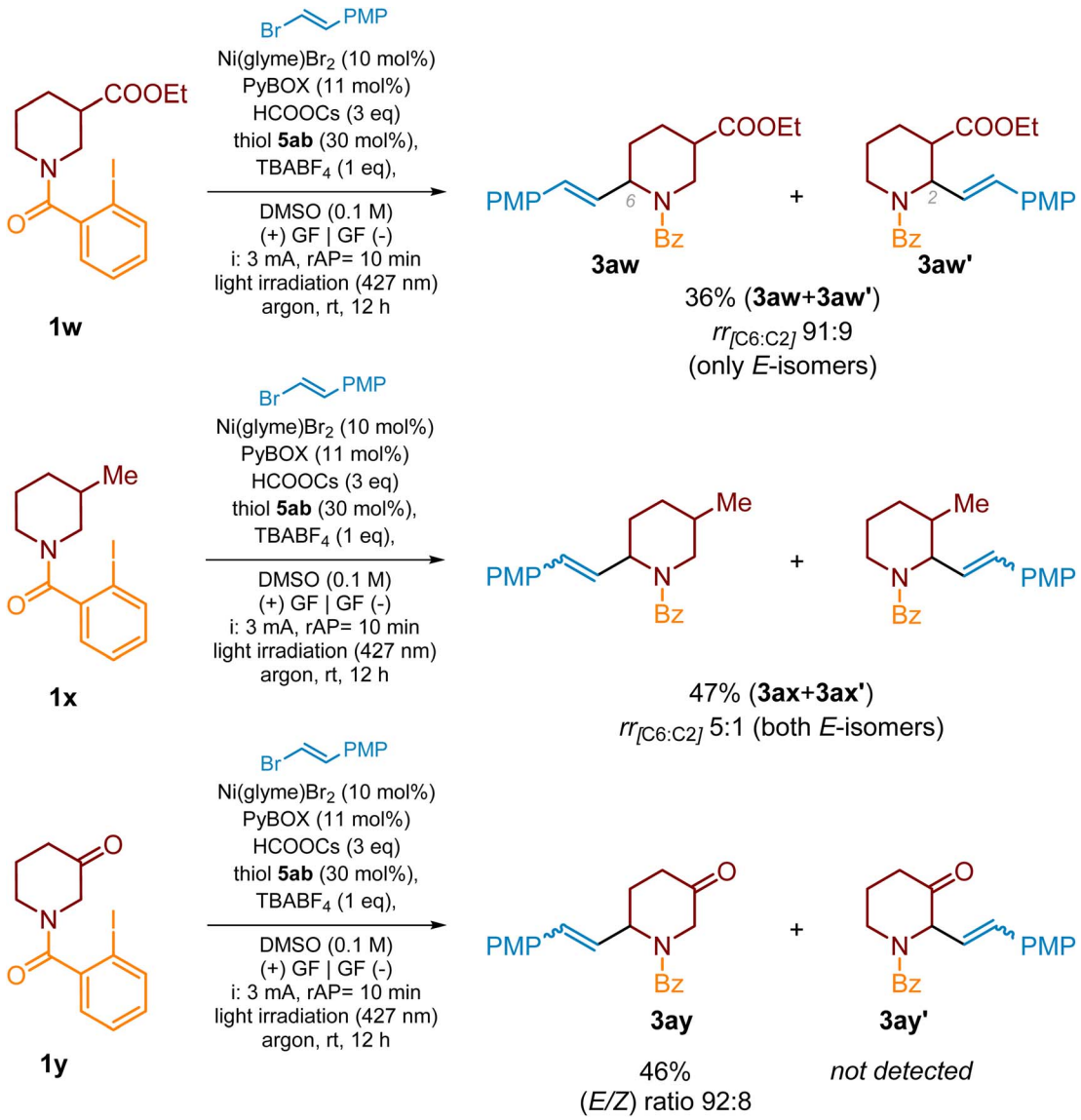

Scheme 6 Remote C–H alkenylation of 3-substituted piperidine scaffolds. The *E*/*Z* ratio of vinyl bromide **2a** was >99 : 1. PMP = 4-methoxyphenyl.

with various heterocyclic scaffolds and model vinyl bromide **2a**. As shown in Scheme 4, C–H alkenylation of a range of 2-iodobenzoyl-protected saturated heterocycles with different ring sizes proceeded smoothly and provided the desired products (*e.g.*, **3ab**, **3al** and **3aq**) smoothly in 72–75% isolated yield. In contrast, alkenylation of the azetidine ring failed (**3as**), and deiodinated azetidine benzamide was obtained as a single product, indicating that the geometry of the 4-membered ring along with its rigidity does not allow for executing the 1,5-HAT process since the distance between the radical center and ring's hydrogen atom is too long.

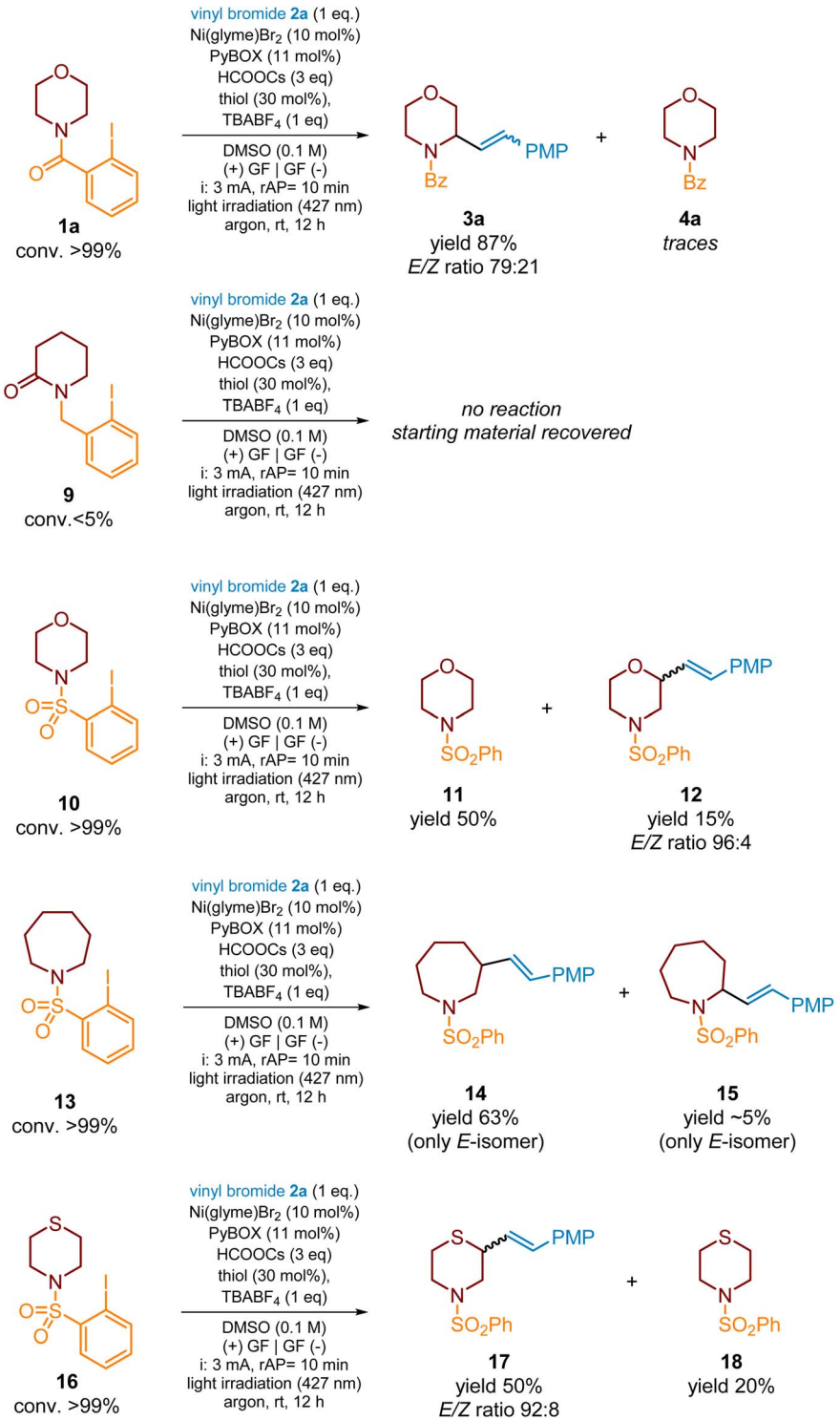

Scheme 7 The effect of a HAT-directing group on C–H alkenylation of morpholine derivatives with vinyl bromide **2a**.

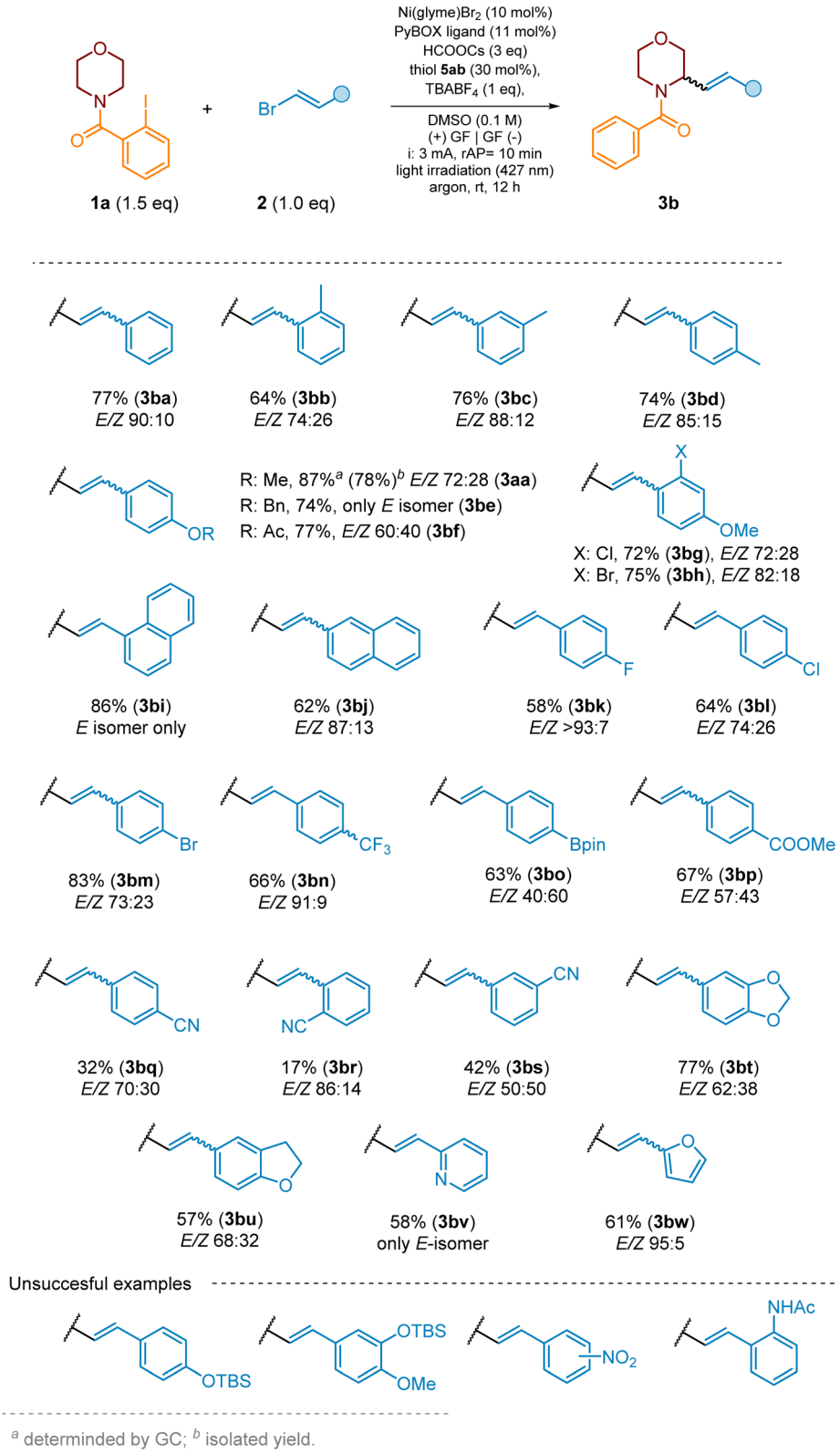

Scheme 8 The scope of vinyl bromides for remote C(sp^3)–H alkenylation of saturated heterocycles. For the *E*/*Z* ratio for starting vinyl bromides please see SI, Section 3.2.

Additional heteroatoms in the ring, like oxygen for **1a** and **1g** or nitrogen in the case of **1d** and **1e** derivatives, did not have a significant influence, and desired products **3aa**, **3ag**, **3ad** and **3ae**, respectively, were obtained in very good yields. Only in the case of alkenylation of thiomorpholine-based benzamide **1c**, the desired product **3ac** was isolated in lower yield (55%),

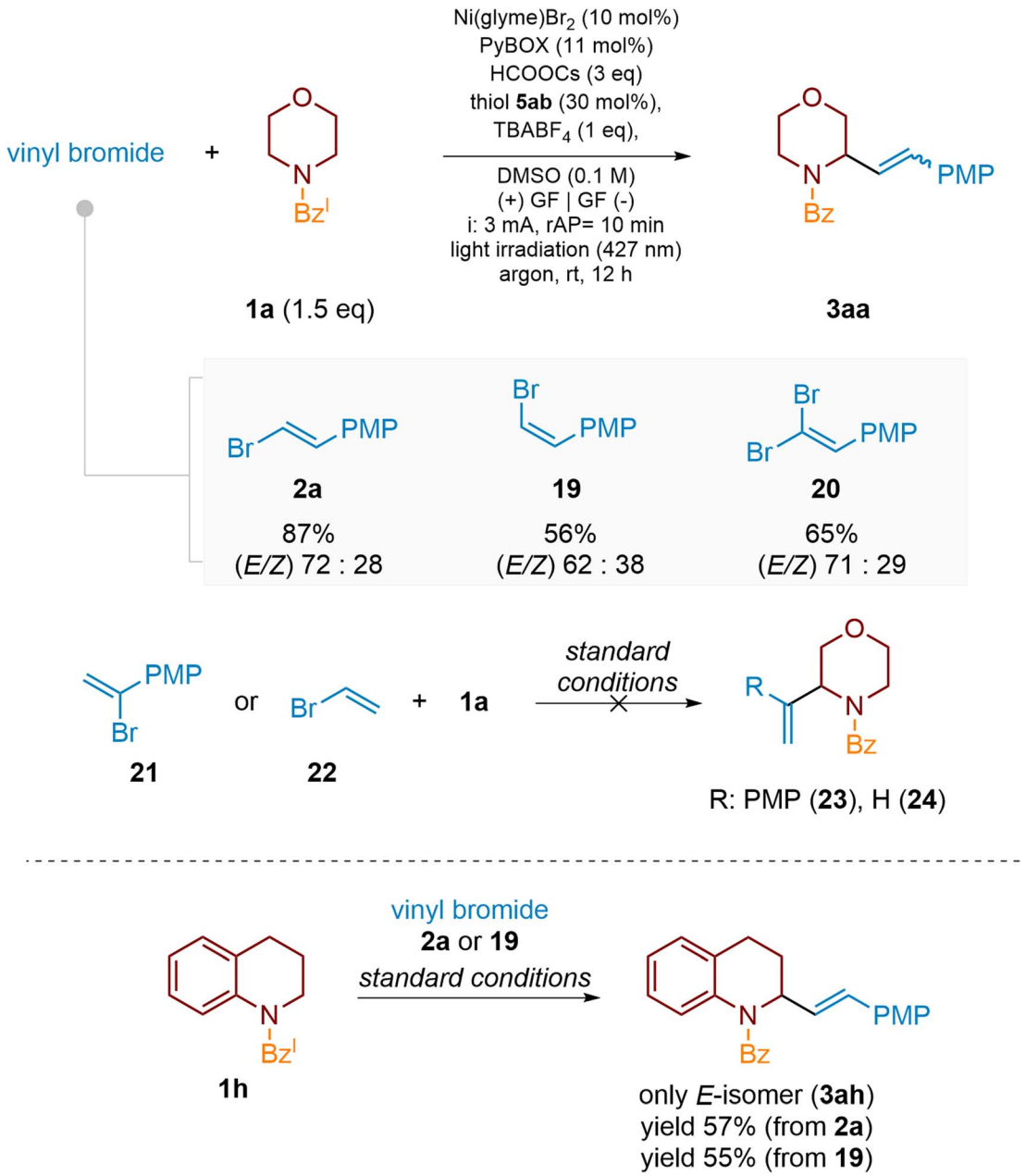

Scheme 9 Reactivity of isomeric vinyl bromides. The *E*/*Z* ratio is >99 : 1 for vinyl bromide **2a** and 1 : 17.5 for vinyl bromide **19**. PMP = 4-methoxyphenyl.

although the starting material was consumed completely. The product **3ac** was accompanied by an increased amount of the deiodinated starting material (~20–30%), indicating a potent issue with the HAT process. We believe that it could be the effect of the change of the 6-membered ring geometry in thiomorpholine due to the presence of the S atom and elongation of the C–S bond lengths compared to C–C (like for piperidine) or C–O (like for morpholine) that may affect the 1,5-HAT transition state geometry decreasing the efficiency of the H-atom translocation. Of course, the alternate negative interactions of the S atom with the Ni-catalyst, which might affect the cross-coupling cycle, cannot be neglected either.

Notably, the alkenylation of monocyclic 6-membered substrates usually proceeded more efficiently than for the corresponding fused analogues (*e.g.*, **3aa** *vs.* **3ak** or **3ab** *vs.* **3ah**), which were often accompanied by a side benzamide product originating from the deiodination of starting 2-iodobenzamide. However, at the same time, all benzofused products (*e.g.*, **3ah**, **3ak**, *etc.*) were formed exclusively as *E*-isomers, whereas for monocyclic substrates the content of the (*Z*)-isomer varied from 2 up to 30%. The potent rationalization of this phenomenon is related to a different conformational dynamic of mono-cyclic and fused heterocyclic scaffolds. It should be expected that reducing the degrees of freedom in fused systems should

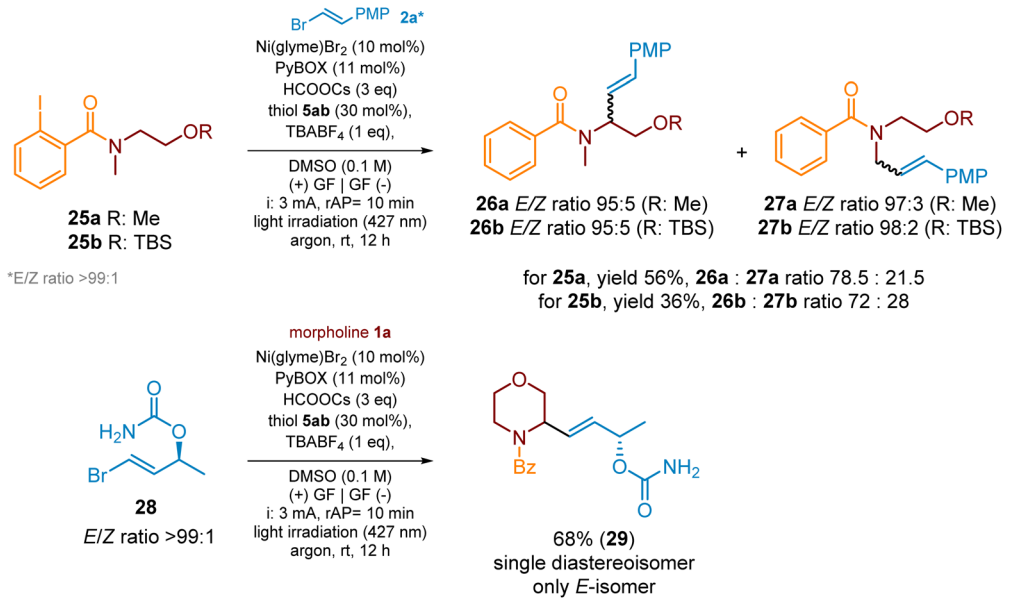

Scheme 10 Remote C–H alkenylation of acyclic amines and alkenylation with 2-alkyl substituted vinyl bromides.

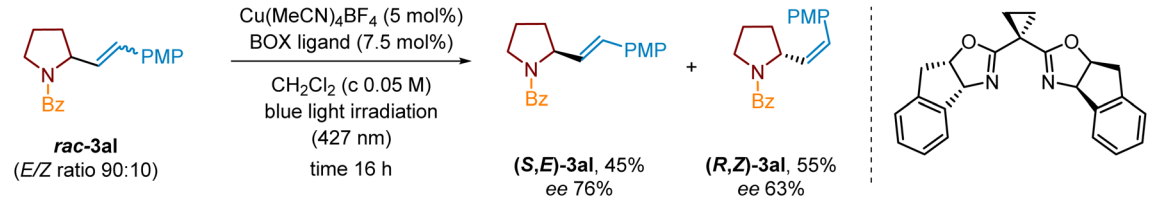

Scheme 11 Photochemical kinetic resolution of pyrrolidine derivative *rac*-3al (*E*/*Z* ratio 90 : 10) in the presence of a chiral Cu/BOX complex.

significantly reduce their conformational dynamics, which will potentially translate into more difficulty in obtaining the appropriate geometry of the transition state of the HAT process. As a result, the rate of the H-atom transfer should decrease, thus providing an opportunity for competitive quenching of the aryl radical to form the corresponding benzamide, which is in accordance with our experimental observations.

For heterocyclic substrates, such as **1i** and **1j**, with two potent positions for H-atom abstraction, the regioselectivity of the HAT reaction was governed by the relative stability of the resulting α-aminoalkyl radical. As presented in Scheme 4, in these cases, the 1,5-HAT step proceeded regioselectively at the C-1 position, resulting in the formation of more stable benzyl-type radical species, and yielded products **3ai** and **3aj**, respectively. Disappointingly, in both cases the yields did not exceed 40% due to the high content of unwanted deiodinated side benzamides (40–60%).

The significance of conformational factors was also strongly manifested in the C–H functionalization of the 5- and 7-membered substrates. As previously mentioned, the alkenylation of the 5-membered pyrrolidine ring (**1l**) proceeded more efficiently than that of the fused analogue, indolidine (**3al** *vs.* **3an**). Furthermore, the flat nature of an oxazolidinone ring (*e.g.*, **3ao**) along with a specific arrangement of the benzoyl group makes the effective orientation of the HAT directing group strongly disfavoured due to an electric repulsion and steric hindrance. As a result, the XAT-generated aryl radical species is incapable of abstraction of any hydrogen atom and is quenched directly, yielding *N*-benzoylated oxazolidinone only. The replacement of a carbonyl group in the oxazolidinone ring (**1o**) with a C(sp^3)-atom (oxazoline **1p**) increased conformational lability of the ring enabling the 1,5-HAT process and yielding compound **3ap** in 50% yield (isol.). Nevertheless, the flexibility of the oxazoline 5-membered ring is still not enough to reach the efficient geometry of the HAT-transition state, compared with 6-membered heterocycles; therefore, again, desired product **3ap** was accompanied by a type-4 side product. Herein, the high ring lability along with entropic factors decreases the probability of the system adopting the optimal geometry of the HAT-transition state that again results in a decrease in the rate of H-atom abstraction promoting side quenching of aryl radical species.

In the case of the alkenylation of benzoazepan-5-one derivative **1r** (product **3ar**), the initial steps, the generation of an aryl radical and the subsequent 1,5-HAT process, proceeded noticeably slower than those for azepane derivative **1q** and other heterocyclic substrates. As a result, after a standard 12 h, product **3ar** was isolated in 39% only and was accompanied by

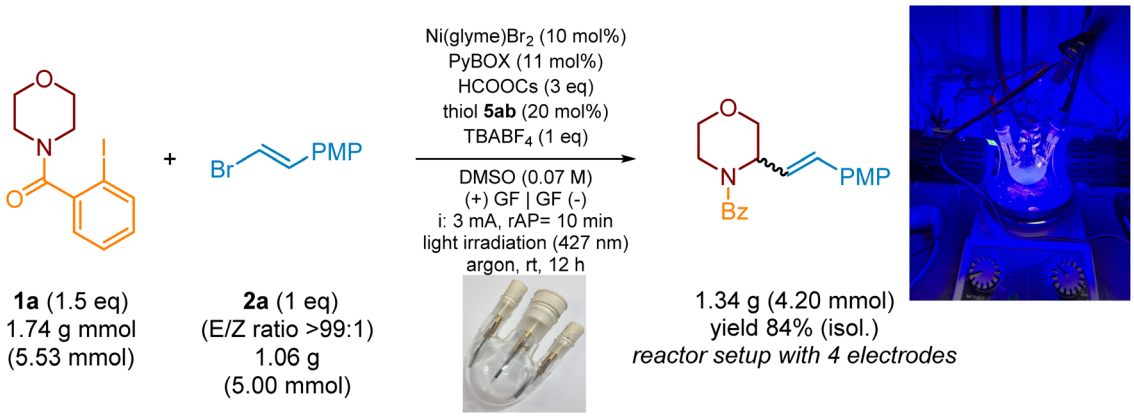

Scheme 12 The large-scale synthesis of compound **3aa**.

a dehalogenated substrate (*ca.* 20%) and numerous vinyl bromide homo-coupling products. Additionally, *ca.* 10–15% of unreacted substrate **1r** was recovered. The reaction proceeded well also for more complex amines, like estrone- and cholesterol-derived substrates, delivering products **3at** and **3au** in good yields and high content of the *E*-isomer (Scheme 4). In both cases a single diastereoisomer was isolated; however, overlapping of diagnostic signals in NMR spectra did not allow relative configuration to be assigned clearly.

Ring substituted heterocycles, *e.g.*, 4-methylpiperidine **1f**, are also suitable substrates for the C–H alkenylation process, as demonstrated in Scheme 4, and, for example, product **3af** was yielded in 74%. An intriguing substrate was piperidin-4-one derivative **1v**. Under standard conditions, beside expected product **3av** (yield 32%), its alkenylation also delivered compound **6** (yield 30%) and a small amount of side-product **4v** (Scheme 5). The product **6** plausibly originated from the oxidation of α-aminoalkyl radical intermediate **7** to the corresponding iminium cation **8** followed by a subsequent base-mediated deprotonation (*e.g.*, by the formate anion) at the C_α-position to the carbonyl group to deliver enamide **6.** Recently, Yatham and co-workers[83] demonstrated synthesis of type-**6** cyclic enamides by a closely related approach involving radical translocation followed by Co-assisted dehydrogenation.

We expected that type **6** enamide could also be formed during the alkenylation of substrate **1w**, bearing ester functionality at the C3 position. However, it was not the case, and this product was not detected in the reaction mixture. On the other hand, this reaction led to the formation of two regioisomeric (*E*)-products **3aw** and **3aw'**, in a ratio of 91 : 9 (Scheme 6). The NMR analysis of the crude reaction mixture revealed only traces of (*Z*)-isomers (<5%). We were not able to separate both regioisomers to confirm the relative configuration. The regioisomeric mixture was also obtained for the alkenylation of 3-methyl-substituted substrate **1x** (Scheme 6, **3ax**/**3ax'** in a ratio of 5 : 1). Again, the C6-alkenylated product was the major one, and only traces of the corresponding (*Z*)-isomers were noticed by a ^{1}H NMR analysis. In contrast, piperidin-3-one derivative **1y** delivered only C6-alkenylated products **3ay** (*E*/*Z*-isomer mixture in a ratio of 92 : 8) in a moderate yield of 46%. For all these cases lower product yields were the effect of side substrate reduction leading to the corresponding benzamides.

Next, using a model morpholine scaffold (Scheme 7), we investigated the scope of a HAT directing group capable of promoting a 1,5-HAT reaction. The 2-iodobenzoyl group outperformed the other two examined functional groups, 2-iodobenzyl and 2-iodobenzosulfonyl, in terms of effective radical translocation through the 1,5-HAT reaction. The 2-iodobenzyl group was completely worthless since it did not deliver an aryl radical through XAT by the $CO_2^{\bullet-}$, under standard reaction conditions. Neither the expected product nor the deiodinated side-product, *N*-benzyl morpholine, was detected in the crude reaction mixtures by the MS analysis. Consequently, only about all of the starting material **9** could be recovered from these experiments. This led us to the conclusion that the electron-deficient character of the HAT directing group is essential for an efficient cleavage of the C(sp^2)–I bond by an XAT reagent.

The reaction of 2-iodobenzosulfonamide **10** delivered primarily deiodinated product **11** (~50%) (Scheme 7). We have also isolated a small quantity of another compound. Its structure was elucidated and indisputably assigned as **12**, according to NMR spectra, including COSY and HSQC correlations (see the SI). The installation of an alkenyl fragment at the C3 position of the morpholine ring indicated that initial H-atom translocation proceeded in the 1,6-manner contrary to all so far studied examples. It is well known that, thanks to the longer length of N–SO_2 and C–SO_2 bonds, sulfamides are capable of promoting 1,6- over 1,5-HAT in acyclic systems.[39,41,44,84–87] However, according to the best of our knowledge, it is the first example of such β-C(sp^3)–H functionalization for the heterocyclic substrate. The low yield of product **12** (~15%, (*E*/*Z*)-isomers mixture in a ratio of 96 : 4) with a simultaneous large content of side-product **11** in the reaction mixture is not surprising considering that the 1,6-HAT process proceeds through a 7-membered transition state and the 6-membered structure of the substrate with its conformational preferences should definitely not favour efficient translocation of the H atom. At this point, we hypothesized that increasing the substrates' ring size should facilitate the 1,6-HAT process thanks to the higher flexibility of such rings. Therefore, to prove this assumption, we prepared

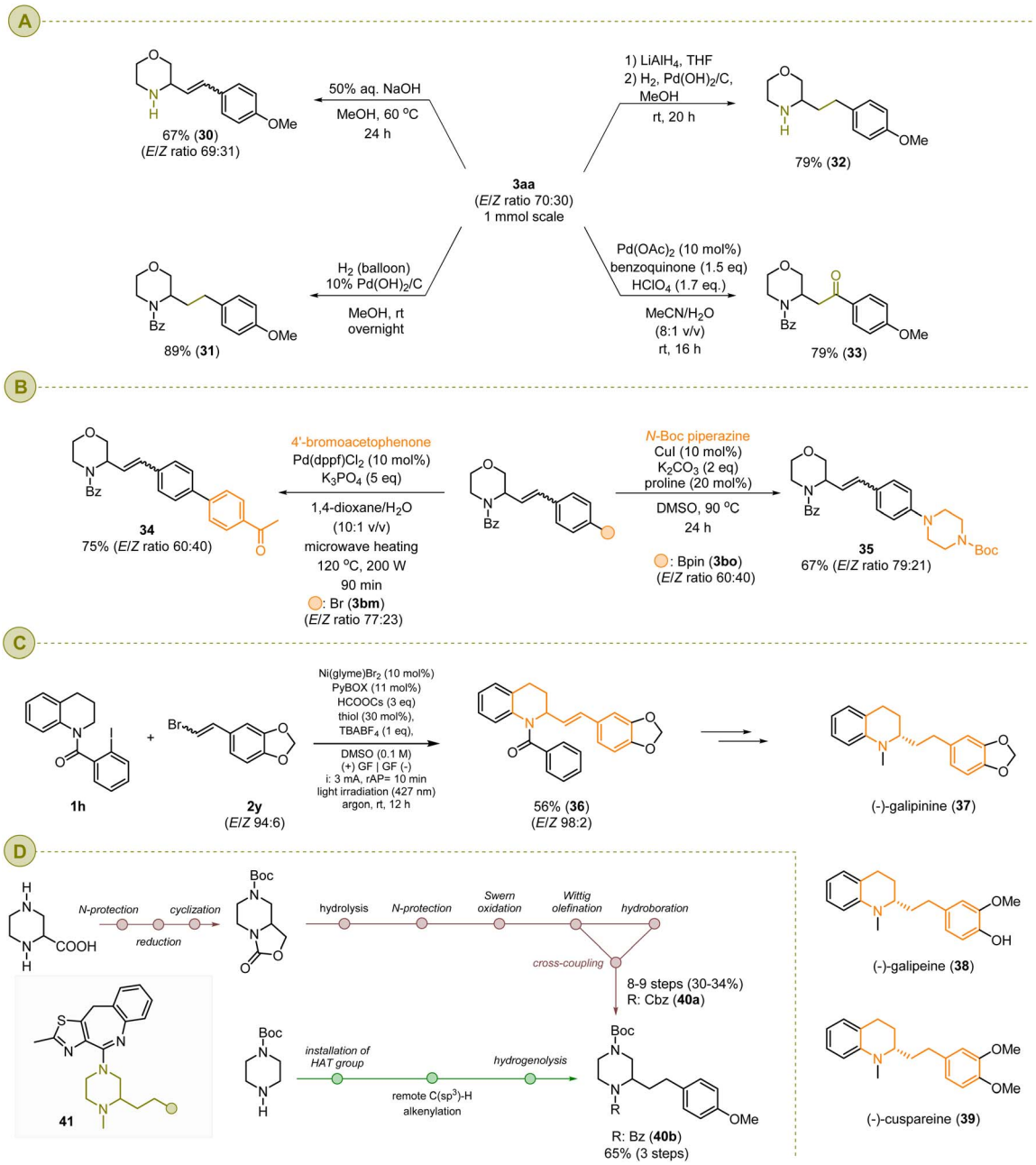

Scheme 13 Synthetic application: (A) functional group transformations; (B) post-functionalization of type-**3** products; (C) synthesis of galipinine precursor **36**; (D) synthetic approach for the preparation of the piperazine fragment of type-**41** bioactive molecules.

azepane benzosulfamide **13** and subjected it to the reaction with model vinyl bromide **2a** under standard photoelectrochemical conditions. As expected, the reaction proceeded with complete conversion of substrate **13** and yielded compound **14** (only the *E*-isomer) in 63%. Notably, deep analysis of the crude reaction mixture revealed the presence of small quantities of the 1,5-HAT-derived product **15** but its yield did not exceed 5%.

The above-presented results encouraged us for one more experiment. As already mentioned, among 6-membered heterocycles, the α-C–H alkenylation of the thiomorpholine ring proceeded in a moderate yield (Scheme 4, **3ac** *vs.* **3aa**, **3ab**, and **3ad–3af**), which was rationalized by a deformation of the 6-membered ring due to the longer length of the C–S bond. On the other side, β-C–H alkenylation of morpholine scaffolds assisted by the 2-iodobenzosulfonyl group yielded product **12** poorly. Therefore, we hypothesized that the replacement of the HAT directing group in the thiomorpholine ring and the combination of both structural effects connected with the presence of the S-atom should enhance the HAT process along with a change of regioselectivity of the C–H functionalization. Indeed, the C–H alkenylation of substrate **16** with model vinyl bromide **2a** yielded expected product **17** in 50% along with side product **18** (20%). The increase in yield from 15% for substrate **12** to 50% for product **17** confirmed the above assumption;

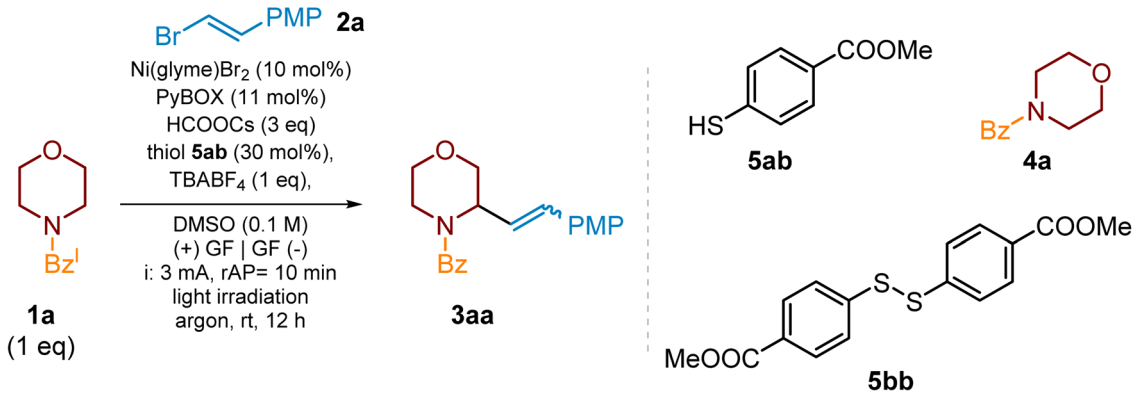

Ent.	Deviation from optimal conditions	Conv. of **1a**[a]	Yield of **3aa**[a]	E/Z ratio
1.	none	>99%	87%	72:28
2.	without light irradiation	>90%[b]	5%	-
3.	without electrolysis (@ 427 nm)	>99%[b]	0%	-
4.	without electrolysis (@ 395 nm)	>90%[b]	>10%	-
5.	without HCOOCs (@ 395 nm)	54%[b]	0%	-
6.	without thiol (@ 427 nm)	38%[b]	6%	80:20
7.	without thiol (@ 395 nm)	75%[b]	6%	79:21
8.	without thiol and formate (@395)	25%[b]	0%	-
9.	disulfide **5bb** instead of **5ab** (@ 395 nm)	>99%	51%	80:20
10.	without argon	>99%	70%	87:13
11.	non-anhydrous DMSO & $HCOOCs{\cdot}H_2O$	87%	22-28%	-
12.	benzamide **4a** instead of **1a**	no reaction	-	-

[a] determined by GC analysis; [b] homocoupling and cross-coupling products assigned by MS:

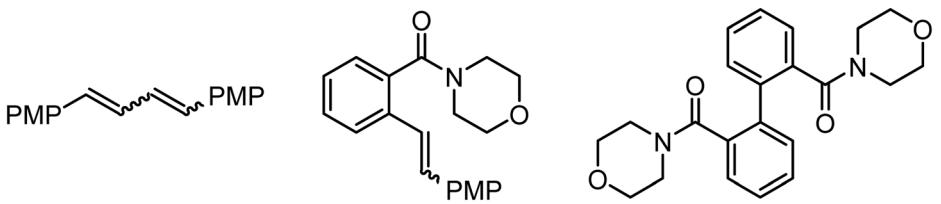

Bz^I = 2-iodobenzoyl; PMP = 4-methoxyphenyl

Scheme 14 Mechanism studies: the exclusion tests and control experiments.

however, the enhancement of HAT is moderate, indicating that the geometry of the transition state is still not the most efficient one.

Subsequently, we investigated the scope of the vinyl bromides in the reaction with morpholine-derived substrate **1a**. The reaction proceeded smoothly for a range of 2-aryl-substituted vinyl bromides bearing both electron-donating and electron-withdrawing groups, indicating very good functional group tolerance (Scheme 8). 2-Aryl vinyl bromides with a nitro group at the phenyl ring did not provide the expected product, plausibly due to potent photoexcitation of the nitro group[88–91] followed by side reactions. The cross-coupling of 2-aryl vinyl bromides with a CN group at various positions of phenyl (**2v–2x**) proceeded less efficiently (products **3bq–3bs**) than for other EWG groups, like ester ones (*e.g.*, **2u**) which yielded product **3bp** in 67%. The reason for this was competitive side radical reactions of the CN group as a radical acceptor,[92,93]

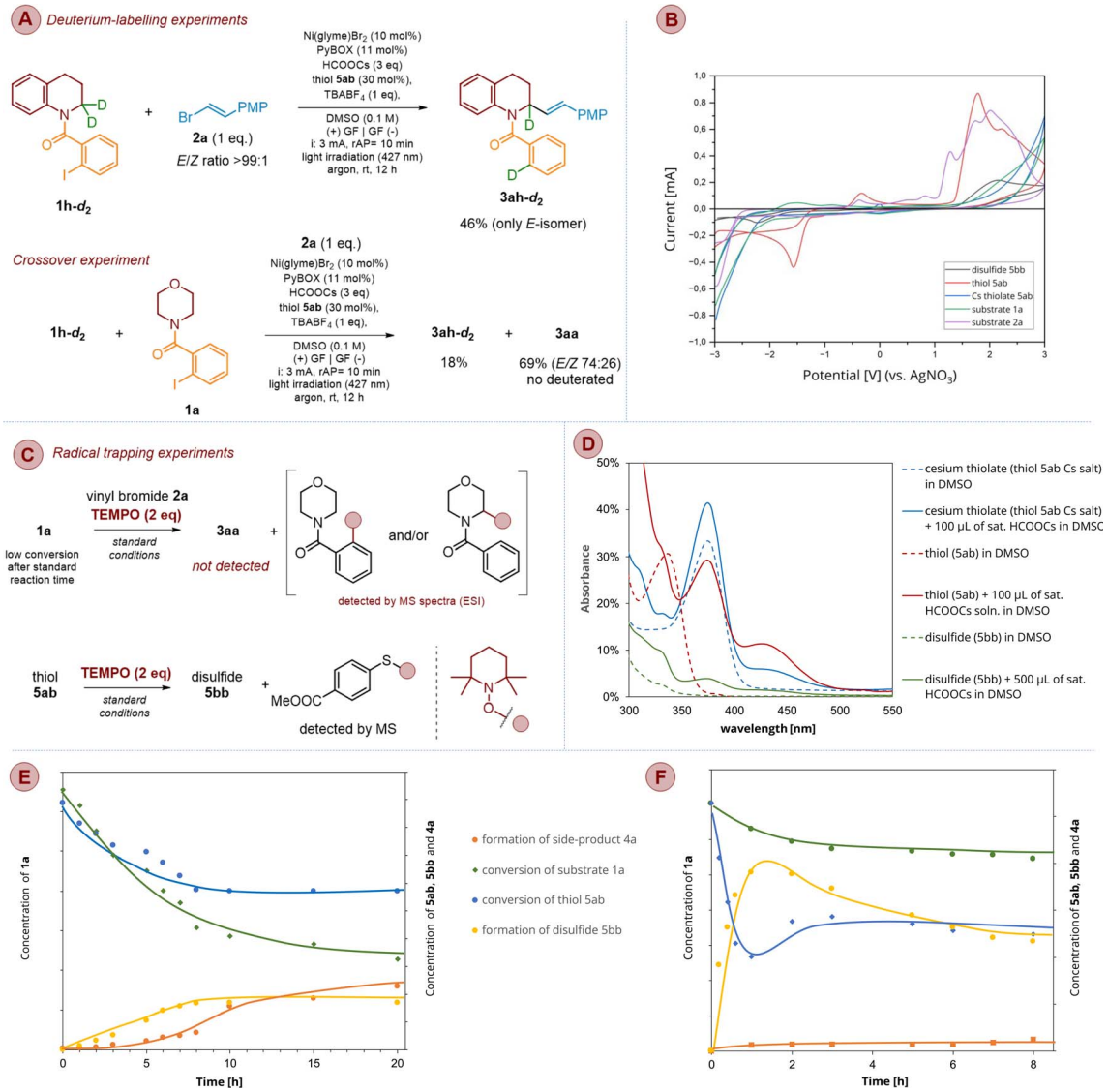

Scheme 15 Mechanistic studies: (A) deuterium-labelling and cross-over experiments; (B) cyclic voltamperograms of key reagents; (C) radical trapping experiments with TEMPO; (D) UV-vis spectra of thiol **5ab**, its Cs salt and disulfide **5bb** with and without addition of HCOOCs in DMSO; (E) kinetic studies of the model reaction without light; (F) kinetic studies of the model reaction (standard conditions).

resulting in low yield of the desired products and a complicated post-reaction mixture.

We were delighted to find that 2-aryl vinyl bromide with a boronic acid ester group can also be efficiently coupled with a morpholine ring (63%), providing product **3bo** for further functionalization *via* standard cross-coupling reactions. Finally, we examined the reactivity of several vinyl bromides bearing heterocyclic rings (**2y–2ab**). As seen in Scheme 8, these reagents were also suitable cross-coupling partners for the investigated reaction sequence, providing desired products (**3bt–3bw**) in 58–77% yield.

In addition to (*E*)-vinyl bromides (**2**), their (*Z*)-isomers (*e.g.*, **19**) may also be used in the examined alkenylation procedure. Scheme 9 shows that for both vinyl bromides, **2a** and **19**, the product **3aa** was obtained as an (*E*/*Z*)-isomer mixture, with the (*E*)-isomer predominating. However, in the case of the (*Z*)-isomer, the cross-coupling proceeded relatively slower, delivering product **3aa** in lower yield after the standard reaction time (12 h). As already mentioned, in contrast to monocyclic amines, the C–H alkenylation of bicyclic heterocycles leads to (*E*)-products only, suggesting that steric effects might prevent subsequent *E*-to-*Z* isomerization. This assumption seems to be supported by other experimental observations presented in Scheme 9. The alkenylation of quinolidine derivative **1h** with (*E*)-vinyl bromide **2a** yielded product **3ah** in 57% as a single (*E*)-isomer. An analogous reaction of **1h** with (*Z*)-vinyl bromide **19** proceeded slightly less efficiently (yield 50%) but delivered the same (*E*)-isomer **3ah**.

Furthermore, vinyl dibromides, *e.g.*, **20**, which served as intermediates in the synthesis of type-**2** substrates, were also suitable for the investigated C–H functionalization and delivered the product **3aa** again with dominance of the (*E*)-isomer

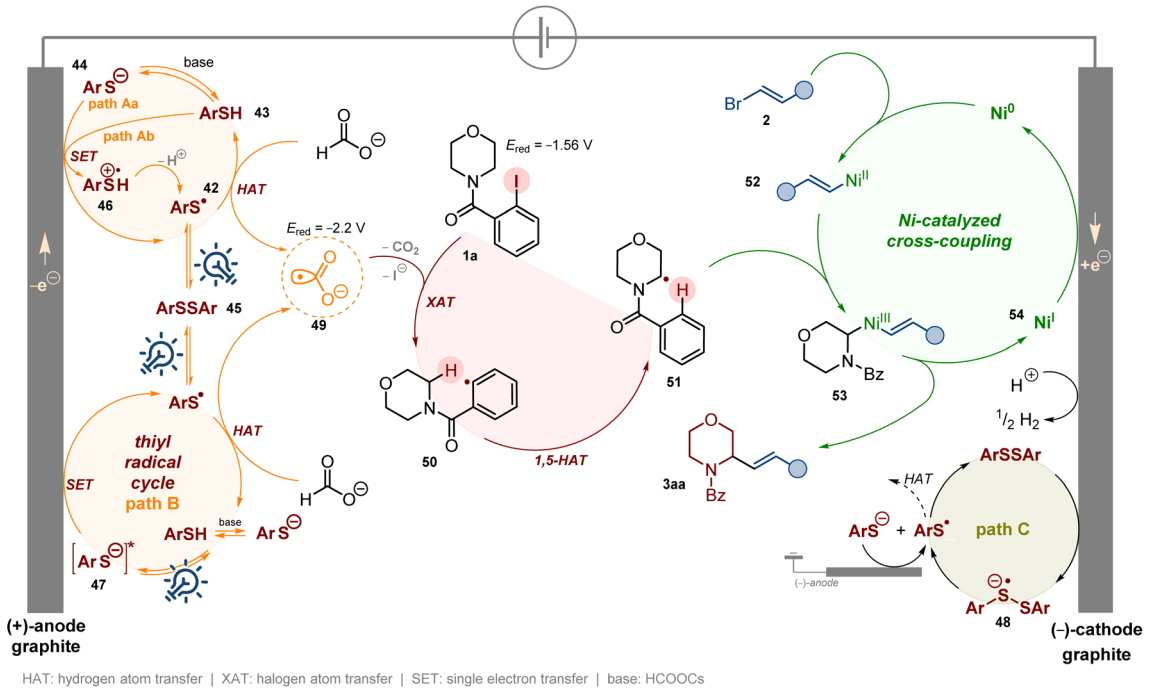

Scheme 16 Proposed mechanism for α-C(sp^3)–H alkenylation of saturated heterocycles.

after the subsequent debromination process under the same reaction conditions. Disappointingly, in contrast to the 2-aryl vinyl bromides presented so far, their sterically more hindered 1-aryl substituted analogues, such as compound **21**, were much less efficient cross-coupling partners and yielded only traces of the desired products (*e.g.*, **23**). The major product was dehalogenated morpholine benzamide **4a**. In addition, the alkenylation of the model substrate **1a** with unsubstituted vinyl bromide **22** was unsuccessful and did not furnish the desired 2-vinylated morpholine **24**.

The developed protocol could also be successfully applied for acyclic amine derivatives, like compounds **25a** and **25b** (Scheme 10). For both cases, the alkenylation with the model vinyl bromide **2a** delivered regioisomeric products **26** and **27** in 56% and 36% yield, respectively. Regioisomers **26a** and **26b** were major products indicating that 1,5-HAT toward the formation of a more stable secondary α-aminoalkyl radical is more preferred. Furthermore, so far used 2-aryl vinyl bromides could be replaced by their alkyl-substituted ones. The reactions with simple 2-alkyl vinyl bromides (see SI, Section 7), under standard reaction conditions, were unsuccessful since, in these cases, the rates of side debromination and homocross-coupling reactions were higher than that of the desired XAT/HAT/cross-coupling sequence. Better results were achieved in the case of more complex vinyl bromides, like compound **28**. The alkenylation of morpholine derivative **1a** with this bromide, under standard conditions, yielded product **29** in 68% as a single diastereoisomer and with (*E*)-geometry of a double bond, as presented in Scheme 10.

Finally, we questioned whether the disclosed procedure could be done in an enantioselective manner by employing chiral Ni complexes. For this purpose, we replaced the so far used PyBOX ligand by its chiral analogues and attempted to perform the reaction between morpholine **1a** and vinyl bromide **2a**. However, since we could not achieve suitable separation of all isomeric products **3aa** during HPLC analysis of the racemic sample, we replaced the model substrate **1a** by pyrrolidine derivative **1l** which was then submitted to alkenylation with vinyl bromide **2a**. Unfortunately, beside numerous chiral PyBOX ligands, we did not observe any asymmetric induction, resulting in the formation of the racemic (*E*)– and (*Z*)-products **3al**, although the overall yields were quite high in all studied cases (see SI, Section 10). The same result was obtained when PyBOX ligands were replaced by a series of chiral BOX ligands (see SI, Section 10).

Contrary to unsuccessful realization of enantioselective mode of C–H alkenylation, we focused on photochemical Cu complex-assisted kinetic resolution following the report by Yuan and Yu.[94] Under reported conditions, racemic pyrrolidine **3al** (*E*/*Z* mixture in a ratio of 90 : 10), in the presence of a chiral Cu-BOX ligand and under blue light irradiation (427 nm), yielded (*S*,*E*)-**3al** and (*R*,*Z*)-**3al** in 45% and 55%, respectively (Scheme 11). Enantiomeric excess for (*S*,*E*)-**3al** was 76%, whereas the optical purity of (*R*,*Z*)-**3al** was 63% ee.

Applications

To explore the practicality of this reaction, a scale-up experiment was carried out under the standard reaction conditions. Initially a reaction of **1a** and **2a** was performed in a 50-mL 3-neck round-bottom flask with angled side arms; however, the desired product **3aa** was obtained in a significantly lower yield (57%, 0.86 g starting from 1.0 g (4.7 mmol) of substrate **2a**)

compared to the same process at the 0.6 mmol scale (see SI, Section 12, Fig. SI-S25). The change of the reactor to a 3-neck round-bottom flask with parallel side arms enhanced the yield to 61%. Finally, placing additional electrodes allowed 1.34 g (84%) of the desired product **3aa** (*E*/*Z* isomer ratio 90 : 10) to be obtained, starting from 1.06 g (5.00 mmol) of vinyl bromide **2a** and 1.74 g (5.53 mmol) of morpholine derivative **1a** (Scheme 12).

To demonstrate the synthetic potential of the alkenylated heterocycles prepared *via* our remote C(sp^3)–H alkenylation conditions, model product **3aa** was subjected to several transformations presented in Scheme 13a. The basic hydrolysis of **3aa** yielded free amine **30** in 67%, and its hydrogenation in the presence of $Pd(OH)_2/C$ yielded product **31** in 89%. Finally, a sequential reduction of amide functionality and hydrogenation of a double bond allowed for synthesis of morpholine **32** in 79% isolated overall yield. The Wacker oxidation of **3aa** delivered ketone **33** in 79%.

The tolerance of the functional group, like halides or boronic acid, provides an extraordinary opportunity to use the resulting products for their late-stage functionalization to deliver complex molecular systems. For example, boronic acid ester **3bo** was readily coupled with aryl halides, like 4′-bromoacetophenone, to furnish product **34** in 75% yield, as demonstrated in Scheme 13b. Notably, varying the aryl halides allows for the late-stage structure diversification of the core fragment, *e.g.*, **1** and **3**, delivering a broad library of products, for instance, for structure–activity relation studies (SARSs), a relatively faster and more efficient way of avoiding time-consuming parallel multistep synthesis. Furthermore, as presented in Scheme 13b, substrate **3bm** can be decorated with an additional heterocyclic scaffold through a Cu-catalyzed Ullmann-type coupling reaction with an *N*-nucleophile, *e.g.*, *N*-Boc piperazine, yielding product **35** in 67%.

Another example of practical application of our alkenylation protocol is the synthesis of compound **36**, which can serve as a precursor of (−)-galipinine **37** (Scheme 13c). The same approach allows for construction of similar tetrahydroquinoline-based alkaloids, like (−)-galipinine (**38**) and (−)-cuspareine (**39**). All of them are isolated from the *Galipea officinalis* shrubby tree, whose trunk bark is used in indigenous folk medicine for its healing properties.[6]

Moreover, as already presented in Scheme 4 and 8, broad substrate scope regarding the vinyl bromides and heterocyclic scaffolds makes our protocol a suitable synthetic tool for rapid and efficient structure diversification either by the already mentioned post-functionalization or by varying both starting materials to differentiate either the heterocyclic core or the side chain. We demonstrated this by synthesizing the piperazine-containing compound **40b**. This functionalized piperazine-based structural motif can be found in numerous naturally occurring compounds or drug candidates,[95–98] like type-**41** compounds widely investigated as potent dopamine receptor antagonists for the treatment of psychotic disorders.[99–102] As shown in Scheme 13d, the already known approach for the synthesis of the core fragment, like compound **40a**, was

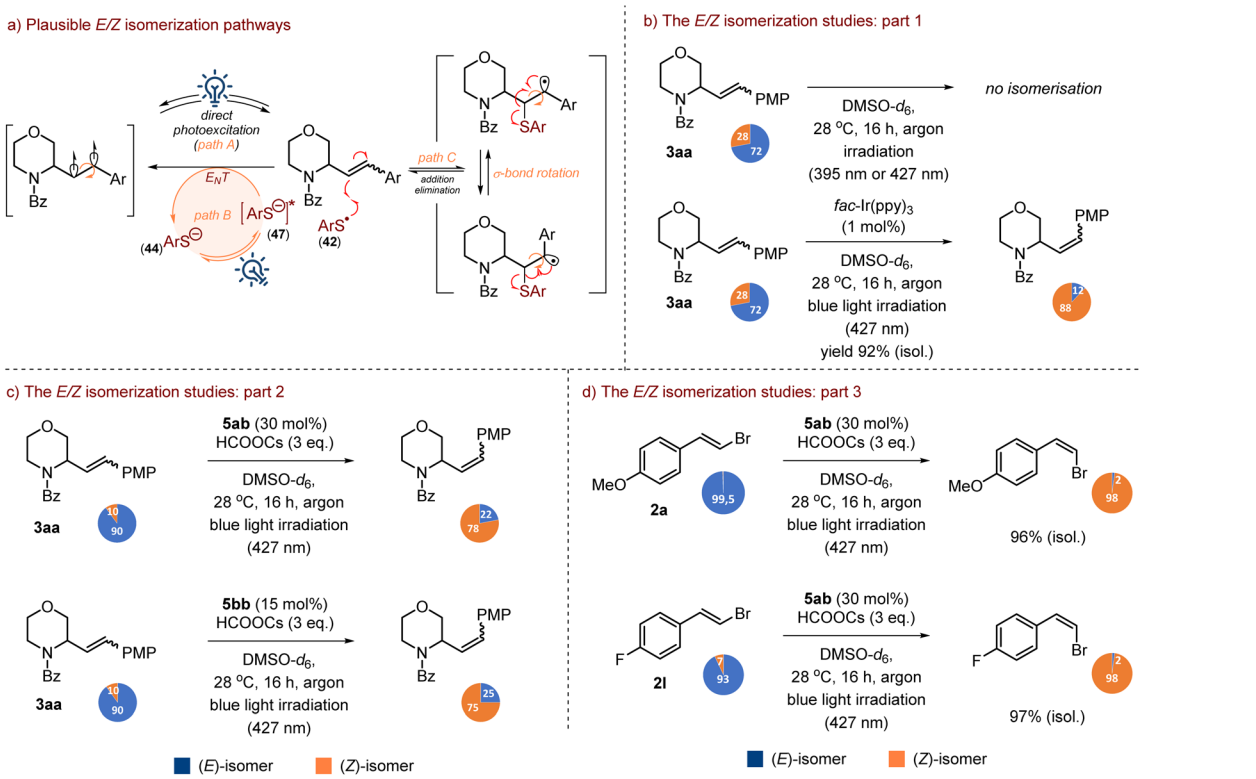

Scheme 17 The *E*/*Z* isomerization studies.

executed in 8–9 steps starting from piperazine-2-carboxylic acid and resulted in an overall yield of 30–33%.[99] No doubt, practical application of this reaction sequence for the preparation of a large library of type-**40a** structures, for instance, for SAR studies, is highly time-consuming which limits its synthetic value. Therefore, we proposed the synthesis of the analogue of **40a**, piperazine **40b** (R: Cbz), from readily available mono-protected piperazine, and included an installation of the HAT directing group, key C(sp^3)–H alkenylation of the heterocyclic ring, and hydrogenation of the double bond. The target product, **40b**, was obtained in 65% overall yield.

Mechanism discussion

To determine the essential parameters of the investigated process, we conducted several control experiments disclosed in Scheme 14.

In the absence of irradiation (Scheme 14, ent. 2), only traces of product **3aa** were noticed (~5%) although the conversion of **1a** was above 90% due to side processes, like homo-coupling of **1a** and cross-coupling of **1a** with **2a** (Scheme 14, bottom), along with slight amounts of the dehalogenated substrate (**4a**). These observations allowed us to draw two conclusions. Firstly, the Ni-catalyzed coupling step does not depend on photochemical conditions. Moreover, since only a catalytic amount of Ni salt is used (10 mol%), the formation of the mentioned by-products proves that electrochemical conditions ensure closure of the Ni-catalytic cycle, restoring key Ni(0) species. Secondly, light is plausibly essential to enable the activation of the substrate, *e.g.*, **1a**, *via* the HAT process.

Without electric current, only traces of product **3aa** and homo/cross-coupling side products were detected along with dominant side-product **4a** (Scheme 14, ent. 3 and 4) regardless of whether blue (427 nm) or purple light (395 nm) was applied. This observation supported the above statement about the essential role of electrolysis in a cross-coupling cycle.

In the control experiment conducted without the addition of formate salt, the conversion of substrate **1a** proceeded very slowly, reaching only 9% after 8 hours. The reaction predominantly yielded homo- and cross-coupling products, as detected by mass spectrometry (Scheme 14, ent. 5). Furthermore, the formation of side product **4a** did not exceed 5–7% even after 12 hours. These results highlight the pivotal role of formate in activating the starting material and demonstrate the absence of other reactive species in the reaction mixture capable of reducing the C(sp^2)–I bond.

When the model reaction was performed without thiol **5ab** under blue light irradiation (427 nm, ent. 6) only 38% conversion of substrate **1a** was noticed along with a slight amount of product (6%, *E*/*Z* is 80 : 20). On the other side, when a light wavelength was changed from 427 to 395 nm (ent. 7), 75% conversion of **1a** was observed but the yield of the desired product **3aa** was at the same level (6%, an *E*/*Z* ratio of 79 : 21). The formation of the slight amount of product in both cases confirms the crucial role of thiol in formation of the XAT reagent. At the same time, the formation of the product indicates the operation of an alternative mechanism delivering the $CO_2^{\bullet-}$ intermediate. This could proceed by a mechanism reported by Yatham and coworkers,[79] postulating the formation of this radical anion directly from formate salt in the presence of a dimsyl anion. Accordingly, they form an EDA-complex which upon purple light irradiation (390 nm) undergoes excitation to produce intermediate $CO_2^{\bullet-}$. Indeed, deep analysis of UV spectra of **1a** + HCOOCs (SI, Fig. SI-5) allows very slight absorption around 370 and 450 nm to be noticed; however, this excitation is too weak to have any influence on the process and can be neglected.

Finally, as indicated in Scheme 14 (ent. 10), the investigated process is slightly air sensitive; the experiments performed without inert gas yielded product **3aa** in *ca.* 70%, whereas under an argon atmosphere, the same product was obtained in 87% (ent. 1). In contrast, the moisture is not allowed, as indicated by control experiments furnishing only traces of the desired product (ent. 11).

Considering that thiyl radicals may also function as hydrogen atom transfer (HAT) reagents, we conducted control experiments to exclude this possibility. Accordingly, compound **4a** was subjected to a reaction with vinyl bromide **2a** under the standard reaction conditions (Scheme 14, ent. 12). After irradiation with blue light and passing an electric current for a standard 12 hours, no formation of the expected product **3aa** was observed. This result indicates that neither ArS$^{\bullet}$ nor $CO_2^{\bullet-}$ acts as a HAT reagent and is incapable of activating our starting material *via* cleavage of the C(sp^3)–H bond.

Deuterium-labelling and crossover experiments indicated that the reaction exclusively underwent intramolecular 1,5-HAT processes, additionally ruling out intermolecular hydrogen atom abstraction (Scheme 15a) and are in agreement with related studies previously reported.[47,55,103]

The addition of a radical trapping reagent, such as TEMPO, effectively inhibited the reaction, and only partial conversion of substrate **1a** was observed. Mass spectrometric analysis of the crude reaction mixture revealed the presence of products resulting from the interception of radical species, specifically, aryl radicals and/or α-aminoalkyl radicals (Scheme 15c, SI and Fig. SI-1a) and aryl thiyl radical (Scheme 15b, SI and Fig. SI-1b), by TEMPO. Notably, the expected product **3aa** was not detected in the crude reaction mixture (see SI, Section 9.1).

The above disclosed observations, along with additional physicochemical measurements, including UV-vis spectra (Scheme 15d, SI, Section 9.3) and CV measurements (Scheme 15b, SI, Section 9.4), allowed us to propose the plausible mechanism that is shown in Scheme 16. The key step is the formation of aryl thiyl radical **42**, a strong HAT reagent,[104] capable of H-atom abstraction from formate salt to deliver highly reducing $CO_2^{\bullet-}$ species **49** ($E_{1/2}$ ($CO_2/CO_2^{\bullet-}$) = −2.2 V).[78,80,105,106] Radical anion **49** reduces substrate **1a** (E_{red} = −1.56 V) *via* the XAT process, furnishing aryl radical **50** capable of the subsequent 1,5-HAT process to afford nucleophilic α-aminoalkyl radical **51**. Meanwhile, vinyl bromide **2a** undergoes oxidative addition with the Ni(0) complex to form Ni(II)-complex **52**. Then, complex **52** intercepts radical **51** to provide Ni(III)-complex **53**. The final reductive elimination furnishes product **3aa** and Ni(I) intermediate **54**. The latter one is then reduced to

Ni(0) to close the Ni-catalytic cycle. This final reduction is realized as a cathodic process, which is essential for the efficiency of the investigated reaction sequence. As already mentioned, without electric current, the product yield cannot exceed 10%, which is equal to the Ni catalyst loading.

We have considered two alternative mechanisms to generate thiyl radical **42** presented in Scheme 16. The first mechanism assumes anodic oxidation of thiol **43** (*via* radical cation **46** following deprotonation, path Aa) or thiolate **44** (path Ab) to thiyl radical **42** which rapidly dimerizes to disulfide **45**. Photoinduced homolysis of the S–S bond in **45** delivers aryl thiyl radical **42** which dimerizes again or reacts with formate, delivering intermediate **49**. At the same time, the resulting disulfide **45** could take one electron from the cathode, leading to disulfide radical anion **48** which decomposes to the thiyl radical **42** and thiolate **44** (path C). The thiolate anion can be converted again to the thiyl radical at the anode and the latter one dimerizes or acts as a HAT reagent.[107,108]

On the other hand, it is a well-known fact that arene thiolate anions, formed by thiol deprotonation with a weak base, may absorb visible light and participate in a photoredox cycle.[109] Therefore, we considered an alternative mechanism, presented in Scheme 16 (path B), in which irradiation of **44** generates excited thiolate **47**, which undergoes a subsequent anodic SET process to deliver thiyl radical **42**.

To determine the mechanism of the generation of radical **42**, we measured UV-vis absorption spectra to detect the light-absorbing species in the reaction mixture (Scheme 15c and SI, Section 9.3). Neither **1a** nor **2a** absorbed visible light in the operational range of 390–430 nm, which eliminated them as potent photoactive species (see SI, Fig. SI-5 and SI-6). The addition of HCOOCs to **1a** provided a slight bathochromic shift of the band, but still the observed absorption was out of the investigated range of wavelengths (see SI, Fig. SI-6). The UV-vis studies also excluded the thiol **5ab** as a photoactive species because its absorbance was also out of the operating light window (λ_{max} 337 nm) (Scheme 15c). As already mentioned, arene thiolate anions may absorb visible light and participate in a photoredox cycle because their HOMO energy is higher than that of the neutral thiol.[109] Indeed, UV spectra of deprotonated thiol **5ab**, obtained by its treatment with Cs_2CO_3, showed a bathochromic shift of absorption to *ca.* 375 nm, along with an increase in absorption intensity (Scheme 15c). Although such absorbance onset overlaps with emission of the employed light source at 395 nm, it does not rationalize why less energetic blue light is also suitable to execute C–H alkenylation efficiently. The answer came after the measurement of the absorption spectrum of thiol **5ab** after the addition of HCOOCs as a base instead of Cs_2CO_3. The recorded spectra showed an almost exact absorption curve with a characteristic red-shifted band at 375 nm (Scheme 15c). However, there was an additional weak band at *ca.* 425 nm, which was missed in the case of cesium thiolate UV-vis data. Finally, when cesium thiolate and HCOOCs were mixed together, the absorption curve was the same as the one for the thiol/HCOOCs mixture, along with similar green emission as shown in Scheme 15d. The appearance of the mentioned band at *ca.* 425 nm suggests that thiolate may also interact with formate anion(s) to give a certain type of donor–acceptor complex that is a photoactive species in the reaction. Noteworthily, the formate salt counterion has no influence on spectroscopic properties of UV spectra, and the same curve was obtained for the thiol mixed with Li, Na, K, Cs, and NH_4 formates and tetra-*n*-butylammonium (TBA) formate (see SI, Fig. SI-12).

To confirm the formation of the excited species **47** and elucidate its role in the proposed mechanism, fluorescence quenching experiments were conducted using photoexcited anion **47**. The addition of varying amounts of the potent quencher, like substrate **1a**, to a mixture of thiol **5ab** and HCOOCs in DMSO did not result in a decrease in emission at either 428 nm (excitation at 375 nm) or 527 nm (excitation at 425 nm). Instead, increasing the concentration of **1a** led to an enhancement of emission intensity, suggesting that **1a** acts as a fluorescence sensitizer or an energy donor, rather than as a quencher. While these findings do not rule out pathway B, they allow us to conclude that the excited anion **47** is not directly involved in the activation of starting materials **1a** and **2a** (see SI, Section 9.3.2).

As previously demonstrated, the C–H alkenylation of **1a** also proceeded when thiol **5ab** was replaced by disulfide **5bb**, affording product **3aa** in 51% yield (Scheme 14, entry 9). Given that disulfides can be readily prepared *via* oxidative coupling of thiols,[110] we hypothesized that similar oxidative coupling could occur under our reaction conditions. Specifically, disulfide **45** is expected to undergo photolysis of its weak S–S bond, generating the key arene thiyl radical **42**. Indeed, the MS and GC analyses of crude reaction mixtures from C–H alkenylation experiments conducted in the presence of thiol **5ab** revealed the presence of disulfide **5bb**, supporting our hypothesis. Furthermore, control experiments in which a DMSO solution of thiol **5ab** was electrolyzed in the presence of $TBABF_4$ as electrolyte confirmed the formation of **5bb** under reaction conditions, which was isolated in 73% yield (see SI, Section 8.4).

As shown in Scheme 14, entry 2, the reaction performed in the absence of light yielded only trace amounts of the desired product, suggesting that the generation of the thiyl radical from disulfide *via* cathodic reduction (path C) either does not occur or proceeds at a rate where dimerization of the thiyl radical outpaces H-atom abstraction. Kinetic experiments appear to support the latter scenario. As shown in Scheme 15e, under dark conditions, substrate **1a** undergoes slow conversion, forming primarily coupling byproducts. Simultaneously, the concentration of thiol **5ab** decreases and stabilizes within approximately 6 hours, while the concentration of disulfide increases to a constant level during the same period. This suggests the establishment of an equilibrium between RSH and RSSR, resulting in insufficient levels of thiyl radical species to promote the designed reaction sequence. Notably, gas chromatography analysis showed only trace amounts (3%) of the desired product after 20 hours.

Upon irradiation of the reaction mixture, the kinetic profile changed significantly (Scheme 15f). In control experiments under blue light irradiation (without formate), the concentration of thiol **5ab** rapidly decreased during the first 60 minutes

and then gradually increased to a stable level after approximately three hours. Concurrently, the concentration of disulfide **5bb** initially increased rapidly, then slightly decreased and stabilized after about three hours.

These observations support two possible hypotheses. The first posits that light irradiation shifts the thiol/disulfide equilibrium by promoting homolytic cleavage of the disulfide S–S bond, thereby generating thiyl radicals. While thiol dimerization continues, photolysis ensures a continuous supply of aryl thiyl radicals, facilitating the generation of $CO_2^{\bullet-}$ and initiating the sequence of XAT, 1,5-HAT, and cross-coupling processes. Alternatively, the second hypothesis suggests that light activates an alternate pathway (such as path B), enabling rapid consumption of thiol, possibly through a rapid anodic oxidation of species **47** to radical **42**. Simultaneously, both paths A and C may operate too, converting the excess of the reactive thiyl radicals into disulfide, which serves as a reservoir and retains their effective concentration to initiate all intended transformations, thereby enabling the formation of C(sp^3)–H alkenylation products. Unfortunately, due to complexity of the entire system, it is not possible to judge undoubtedly which pathway, A or B, dominates; therefore, it seems to be more appropriate to assume that both paths operate simultaneously along with cathodic transformations of disulfide (path C).

The last issue was the explanation of partial (*E*/*Z*)-isomerization of the C–H alkenylation for some products, although, in all examined cases pure (*E*)-isomers of vinyl bromides were used. Since our protocol does not use any of the common metal-based or organic photocatalysts, we considered two possible scenarios of observed double bond isomerization: (1) direct excitation of a double bond to a diradical (path A) or (2) reactive species-promoted isomerization *via* either triplet energy transfer (path B)[111,112] or an addition/elimination sequence (path C), as shown in Scheme 17a.[104] Moreover, the isomerization can either be a primary or secondary process depending on whether it deals with a substrate, vinyl bromide, or product.

The initial control experiments, in which it was directly irradiated with either purple (395 nm) or blue light (427 nm) excluded path A, since blue (427 nm) or purple (395 nm) light irradiation of a solution of **3aa** (*E*/*Z* ratio 72 : 28) in DMSO did not result in any change in the isomer ratio after 16 hours (Scheme 17b, eqn 1). In contrast, in the control experiment, we have added *fac*-Ir(ppy)$_3$ to the solution of **3aa** in DMSO, and the resulting mixture was irradiated with blue light (427 nm). After 16 hours, an initial (*E*/*Z*)-isomer ratio of 72 : 28 changed leading predominately to a contra-thermodynamic (*Z*)-isomer (*E*/*Z* ratio of 12 : 88) which was isolated in 92% yield (Scheme 17b, eqn 2).

Based on these two observations, additional control experiments were performed to determine the mechanism (path B or C) and identify active species involved in the isomerization process. In particular, we focused on the arene thiyl radical as a potent isomerisation agent.[104] Blue light irradiation (427 nm) of a solution of (*E*/*Z*)-**3aa**, thiol **5ab** (30 mol%) and HCOOCs (3 equiv.) in DMSO resulted in a significant change in the (*E*/*Z*)-ratio from 90 : 10 to 22 : 78, after 16 h, with a dominance of the (*Z*)-isomer (Scheme 17c, eqn 1). The same outcome was observed when thiol **5ab** was replaced by disulfide **5bb** (15 mol%). After standard time, 16 h, again the *E*/*Z*-isomer ratio changed from 90 : 10 to 25 : 75 (Scheme 17c, eqn 2). As can be seen from the data collected in Scheme 4, the tendency for the partial formation of type-(*Z*)-**3** products was noticed only for mono-cyclic substrates **1**, which may suggest that *E*-to-Z isomerisation of a double bond is easier for them due to their less steric hindrance and better accessibility to the double bond compared to fused systems. Furthermore, as disclosed in Scheme 8, the electronic nature of aryl groups of vinyl bromides did not have a significant influence on the (*E*/*Z*)-isomer ratio of the product, and partial isomerisation was observed for both electron-rich and electron-poor systems, without any strict trends. This again confirms our statement about the pivotal role of steric factors on the final isomer ratio. As further experiments revealed, the starting (*E*)-vinyl bromides, *e.g.*, **2a** and **2l**, can also be isomerized to (*Z*)-isomers in the presence of thiol and formate salt (Scheme 17d, eqn 1 & 2). The isomerization proceeded smoothly for electron-rich systems, like **2a**, and electron-deficient systems, such as bromide **2l**.

It is important to emphasize that the isomerization our products, *e.g.*, **3aa**, occurred only in the presence of HCOOCs. Otherwise, the (*E*/*Z*)-isomer ratio became almost unchanged (see SI, Section 8.2). The same was observed in the cases when the mixture of (*E*/*Z*)-**3aa** and HCOOCs without thiol or disulfide was exposed to blue light irradiation. This corresponds to our UV-vis studies, which revealed that neither thiol **5ab** nor disulfide **5bb** absorbs the blue light with a wavelength of 427 nm. This again confirms the pivotal role of formate salt in the investigated process, not only as a precursor for the XAT reagent (CO_2 radical anion) but also as an essential activator for the generation of the thiyl radical either from thiol or disulfide.

Analysis of the mass spectra of crude reaction mixtures from the isomerization experiments, as depicted in Scheme 17c and d, revealed the presence of very weak mass peaks potentially corresponding to aryl thiyl addition/hydrogen atom transfer (HAT) reaction products. The formation of these species appears to support our hypothesis regarding thiyl radical-induced double bond isomerization *via* an addition/elimination mechanism (path C) and is consistent with previous reports.[104]

To assess the plausibility of isomerization proceeding through the path B mechanism, fluorescence quenching experiments involving the excited thiolate species (**47**) were conducted. Emission spectra recorded upon excitation at 375 nm and 425 nm (see SI, Fig. SI-14) indicated that compound **3aa** could act as a potent quencher of the excited species **47**, although quenching was relatively weak, especially with excitation at a lower energy wavelength. This observation suggests that a significant interaction between species **47** and the product (or vinyl bromide) under the reaction conditions cannot be excluded, potentially facilitating double bond activation to a diradical species, for example, *via* an energy transfer process as illustrated in Scheme 17a.

Nevertheless, the limited amount of currently available data, along with the inherent complexity of the reaction system, precludes unequivocal and definitive proof of isomerization *via* path B. Therefore, we are more inclined to attribute the

observed partial isomerization of the products to path C as the most probable mechanism.

Conclusions

In summary, we developed a general and mild photoelectrochemical method for α- or β-C(sp^3)–H alkenylation of various readily available monocyclic or benzofused amines using a series of vinyl bromides. The established protocol accommodates a wide variety of amine scaffolds and vinyl bromides, demonstrates tolerance for different functional groups, exhibits adequate *E*/*Z* selectivity, and shows slight sensitivity to oxygen. An Ni complex catalyses the installation of an alkenyl fragment, which results in limited compatibility with moisture. Mechanistic studies suggest that the transformation relies on the formation of aryl thiyl radical species, which react with formate to yield $CO_2^{\bullet-}$. This species acts as an XAT reagent capable of generating an aryl radical from the corresponding aryl iodide. Subsequently, the aryl radical abstracts an H-atom from the amine fragment through intramolecular 1,5-HAT, resulting in the formation of an α-aminoalkyl radical, which is then intercepted by the Ni-alkenyl complex. Furthermore, we demonstrated that substituting the 2-iodobenzoyl HAT-directing group with its sulfonyl analogue facilitates a 1,6-HAT process, leading to β-alkenylated products. This method has shown significant applicability in the construction of complex heterocyclic scaffolds and in the late-stage functionalisation of bioactive molecules. Additionally, the resulting allyl- and homoallyl amine products can be readily transformed into various α- and β-functionalised cyclic amines, thereby facilitating the synthesis of numerous nitrogen-containing heterocyclic natural products and pharmacoactive compounds. Consequently, the reported procedure is anticipated to have numerous applications in synthetic organic chemistry and medicinal chemistry, including drug discovery studies.

Methods

In a glove box, an oven dried ElectraSyn vial (A) (10 mL) equipped with a magnetic stir bar was charged with vinyl bromide (0.6 mmol, 1.0 equiv.), 2-halobenzamide (0.66 mmol, 1.1 equiv.), HCOOCs (1.8 mmol, 3.0 equiv.), methyl 4-mercaptobenzoate **5ab** (0.12 mmol, 0.2 equiv.) and *n*-Bu_4NBF_6 (0.6 mmol, 1.0 equiv.). The vial was closed with a PTFE cap equipped with an anode (graphite) and a cathode (graphite). Another oven dried 5 mL vial (B) was charged with Ni(glyme)Br_2 (0.06 mmol, 0.1 equiv.) and PyBOX ligand **L8a** (0.066 mmol, 0.11 equiv.). A magnetic stir bar was added and vial B was closed with a septa cap. Both vials were taken out from the glove box and kept under argon. Under argon 4 mL dry DMSO was added to both vials; 4 mL to the vial A and 2 mL to the vial B. The mixture in the vial B was continuously stirred at 60 °C for 10 min to prepare the pre–nickel complex. After that, solution of the Ni-complex was transferred from the vial B to the vial A. Now, the vial A was installed on an ElectraSyn stand and electrolysis was started (constant current 3 mA, time 12 h, and polarity of alternating electrodes was changed every 10 min) along with blue light irradiation using a Kessil™ LED lamp (427 nm, 5 cm away, with a cooling fan to keep the reaction temperature at 25 °C) for 12 h. After completion of the reaction, the reaction mixture was transferred to a separatory funnel; the electrodes were rinsed with ethyl acetate (5 mL) and water. The aqueous layer was extracted with ethyl acetate (3 × 20 mL). The combined organics were washed successively with brine (1 × 30 mL) and then dried over $MgSO_4$ or Na_2SO_4. After removal of the drying agent, solvents and volatiles were removed on a rotary evaporator. The crude product was purified by automated flash chromatography. The obtained product was kept under high vacuum (10^{-3} bar) at 70 °C in the Kugelrohr apparatus for 10 h to remove the traces of solvents. The progress of the reaction was followed by TLC by using UV (254 nm) detection and vanillin stain. The *E*/*Z*-isomer ratio was determined by ^{1}H NMR or GC analysis.

Author contributions

Siddharth K. Dave: synthesis of starting materials, optimization studies, scope studies, application studies, characterization of chemical compounds, mechanism studies, manuscript preparation. Sebastian Stecko: project concept, preliminary studies, synthesis of selected compounds, scope studies, UV-vis, CV, fluorescence measurements, data analysis, manuscript preparation, mechanism studies, constructor of the required equipment.

Conflicts of interest

The authors declare no conflict of interest.

Data availability

The data supporting this article have been included as part of the supplementary information (SI). Supplementary information: all experimental setup and details, materials used, the optimization process of remote C–H alkenylation of amines, mechanistic studies, synthetic procedures, the 1H, 13C, and 19F NMR characterization data of the products, equipment setup, optimisation studies, characterisation of organic compounds, photochemical studies, and copies of 1H, 13C, and 19F NMR spectra. See DOI: https://doi.org/10.1039/d5sc08559d.

Acknowledgements

The authors are grateful to the National Science Center of Poland for financial support through a research grant (OPUS 2021/43/B/ST4/019115).

References

1 A.-j. Deng and H.-l. Qin, *Phytochemistry*, 2010, **71**, 816–822.
2 P. Huang, P. Cheng, M. Sun, X. Liu, Z. Qing, Y. Liu, Z. Yang, H. Liu, C. Li and J. Zeng, *Med. Plant Biol.*, 2024, **3**, e020.
3 X. Luo, L. Pedro, V. Milic, S. Mulhovo, A. Duarte, N. Duarte and M.-J. U. Ferreira, *Planta Med.*, 2012, **78**, 148–153.

4 X. Luo, D. Pires, J. A. Aínsa, B. Gracia, N. Duarte, S. Mulhovo, E. Anes and M.-J. U. Ferreira, *J. Ethnopharm.*, 2013, **146**, 417–422.
5 Y. G. Xia, G. Y. Li, J. Liang, B. Y. Yang, S. W. Lü and H. X. Kuang, *Evid. Based. Complement. Alternat. Med.*, 2014, **2014**, 684508.
6 S. G. Davies, A. M. Fletcher, I. T. T. Houlsby, P. M. Roberts, J. E. Thomson and D. Zimmer, *J. Nat. Prod.*, 2018, **81**, 2731–2742.
7 I. Jacquemond-Collet, F. Benoit-Vical, A. Valentin, E. Stanislas, M. Mallié and I. Fourasté, *Planta Med.*, 2002, **68**, 68–69.
8 A. J. Aladesanmi, C. J. Kelley and J. D. Leary, *J. Nat. Prod.*, 1983, **46**, 127–131.
9 E. Tojo, M. A. Önür, A. J. Freyer and M. Shamma, *J. Nat. Prod.*, 1990, **53**, 634–637.
10 S. Dayot, D. Speisky, A. Couvelard, P. Bourgoin, V. Gratio, J. Cros, V. Rebours, A. Sauvanet, P. Bedossa, V. Paradis, P. Ruszniewski, A. Couvineau and T. Voisin, *Oncotarget*, 2018, **9**, 6952–6967.
11 P. Malherbe, E. Borroni, E. Pinard, J. G. Wettstein and F. Knoflach, *Mol. Pharm.*, 2009, **76**, 618–631.
12 *DrugBank.com: Iferanserin*, https://go.drugbank.com/drugs/DB11686.
13 *DrugBank.com: Encainide*, https://go.drugbank.com/drugs/DB01228.
14 M. J. Antonaccio, A. W. Gomoll and J. E. Byrne, *Cardiovasc. Drugs Ther.*, 1989, **3**, 691–710.
15 R. L. Grange, E. A. Clizbe and P. A. Evans, *Synthesis*, 2016, **48**, 2911–2968.
16 A. K. Mailyan, J. A. Eickhoff, A. S. Minakova, Z. Gu, P. Lu and A. Zakarian, *Chem. Rev.*, 2016, **116**, 4441–4557.
17 S. L. Rössler, D. A. Petrone and E. M. Carreira, *Acc. Chem. Res.*, 2019, **52**, 2657–2672.
18 Q. Cheng, H.-F. Tu, C. Zheng, J.-P. Qu, G. Helmchen and S.-L. You, *Chem. Rev.*, 2019, **119**, 1855–1969.
19 O. Pàmies, J. Margalef, S. Cañellas, J. James, E. Judge, P. J. Guiry, C. Moberg, J.-E. Bäckvall, A. Pfaltz, M. A. Pericàs and M. Diéguez, *Chem. Rev.*, 2021, **121**, 4373–4505.
20 Y. Huang, R.-Z. Huang and Y. Zhao, *J. Am. Chem. Soc.*, 2016, **138**, 6571–6576.
21 B. M. Trost, C.-I. Hung and G. Mata, *Angew. Chem., Int. Ed.*, 2020, **59**, 4240–4261.
22 O. I. Afanasyev, E. Kuchuk, D. L. Usanov and D. Chusov, *Chem. Rev.*, 2019, **119**, 11857–11911.
23 R. A. Fernandes, P. Kattanguru, S. P. Gholap and D. A. Chaudhari, *Org. Biomol. Chem.*, 2017, **15**, 2672–2710.
24 Y. Ichikawa, *Synlett*, 2007, **2007**, 2927–2936.
25 P.-A. Nocquet, S. Henrion, A. Macé, B. Carboni, J. M. Villalgordo and F. Carreaux, *Eur. J. Org Chem.*, 2017, **2017**, 1295–1307.
26 R. Karl Dieter and R. R. Sharma, *Tetrahedron Lett.*, 1997, **38**, 5937–5940.
27 R. K. Dieter, C. M. Topping, K. R. Chandupatla and K. Lu, *J. Am. Chem. Soc.*, 2001, **123**, 5132–5133.
28 D. Antermite and J. A. Bull, *Synthesis*, 2019, **51**, 3171–3204.
29 E. N. Bahena, S. E. Griffin and L. L. Schafer, *J. Am. Chem. Soc.*, 2020, **142**, 20566–20571.
30 L. Li, Y.-C. Liu and H. Shi, *J. Am. Chem. Soc.*, 2021, **143**, 4154–4161.
31 A. L. Krasovskiy, S. Haley, K. Voigtritter and B. H. Lipshutz, *Org. Lett.*, 2014, **16**, 4066–4069.
32 E. Bisz, M. Koston and M. Szostak, *Green Chem.*, 2021, **23**, 7515–7521.
33 R. N. Shakhmaev, A. S. Sunagatullina and V. V. Zorin, *Russ. J. Org. Chem.*, 2014, **50**, 322–331.
34 M. Garbacz and S. Stecko, *Org. Biomol. Chem.*, 2021, **19**, 8578–8585.
35 M. Garbacz and S. Stecko, *Org. Biomol. Chem.*, 2023, **21**, 115–126.
36 A. Noble and D. W. C. MacMillan, *J. Am. Chem. Soc.*, 2014, **136**, 11602–11605.
37 Y.-T. Wang, Y.-L. Shih, Y.-K. Wu and I. Ryu, *Adv. Synth. Catal.*, 2022, **364**, 1039–1043.
38 Z. Qing, H. Cao, P. Cheng, W. Wang, J. Zeng and H. Xie, *Org. Chem. Front.*, 2018, **5**, 353–357.
39 M. Nechab, S. Mondal and M. P. Bertrand, *Chem.–Eur. J.*, 2014, **20**, 16034–16059.
40 W. Guo, Q. Wang and J. Zhu, *Chem. Soc. Rev.*, 2021, **50**, 7359–7377.
41 L. Capaldo, D. Ravelli and M. Fagnoni, *Chem. Rev.*, 2022, **122**, 1875–1924.
42 L. Capaldo and D. Ravelli, *Eur. J. Org Chem.*, 2017, **2017**, 2056–2071.
43 W. Li and C. Zhu, Radically Initiated Distal C(sp^3)–H Functionalization, in *Remote C-H Bond Functionalizations*, ed. D. Maiti and S. Guin Wiley & Sons, New York 2021.
44 S. Sarkar, K. P. S. Cheung and V. Gevorgyan, *Chem. Sci.*, 2020, **11**, 12974–12993.
45 L. M. Stateman, K. M. Nakafuku and D. A. Nagib, *Synthesis*, 2018, **50**, 1569–1586.
46 S. Sarkar, S. Wagulde, X. Jia and V. Gevorgyan, *Chem*, 2022, **8**, 3096–3108.
47 R. Guo, H. Xiao, S. Li, Y. Luo, J. Bai, M. Zhang, Y. Guo, X. Qi and G. Zhang, *Angew. Chem., Int. Ed.*, 2022, **61**, e202208232.
48 J. Wang, Q. Xie, G. Gao, H. Li, W. Lu, X. Cai, X. Chen and B. Huang, *Org. Chem. Front.*, 2023, **10**, 4394–4399.
49 M. G. Pizzio, E. G. Mata, P. Dauban and T. Saget, *Eur. J. Org Chem.*, 2023, **26**, e202300616.
50 V. Srinivasu, K. Pal, S. Giri and D. Sureshkumar, *Org. Lett.*, 2024, **26**, 10328–10333.
51 Z. Lei, W. Zhang and J. Wu, *ACS Catal.*, 2023, **13**, 16105–16113.
52 X. Lin, H. Huang, F. Yang, Y. Ren, Y. Gao and W. Su, *Org. Chem. Front.*, 2025, **12**, 829–837.
53 J. Zheng, H. Zhang, S. Kong, Y. Ma, Q. Du, B. Yi, G. Zhang and R. Guo, *ACS Catal.*, 2024, **14**, 1725–1732.
54 H. Zhang, W. Gu, Q. Li, J. Zheng, J. Xiao, Y. Kang, W. Kandegama, X. Qi, G. Zhang and R. Guo, *ACS Catal.*, 2025, **15**, 15425–15434.
55 J. Lu, K. Yuan, J. Zheng, H. Zhang, S. Chen, J. Ma, X. Liu, B. Tu, G. Zhang and R. Guo, *Angew. Chem., Int. Ed.*, 2024, **63**, e202409310.

56 M. Garbacz and S. Stecko, *Adv. Synth. Catal.*, 2020, **362**, 3213–3222.
57 S. K. Kariofillis, B. J. Shields, M. A. Tekle-Smith, M. J. Zacuto and A. G. Doyle, *J. Am. Chem. Soc.*, 2020, **142**, 7683–7689.
58 A. Q. Cusumano, B. C. Chaffin and A. G. Doyle, *J. Am. Chem. Soc.*, 2024, **146**, 15331–15344.
59 X.-C. He, K.-R. Li, J. Gao, J.-P. Guan, H.-B. Chen, H.-Y. Xiang, K. Chen and H. Yang, *Org. Lett.*, 2023, **25**, 4056–4060.
60 T. Constantin, F. Juliá, N. S. Sheikh and D. Leonori, *Chem. Sci.*, 2020, **11**, 12822–12828.
61 Z. Li, W. Yan, X. Zhou, C. Yang, L. Guo and W. Xia, *Org. Chem. Front.*, 2025, **12**, 4946–4955.
62 D. Kobus-Bartoszewicz, M. Zalewski, K. Melcer, M. Warda and S. Stecko, *Adv. Synth. Catal.*, 2025, **367**, e202401326.
63 S. Wang, C. Yang, S. Sun and J. Wang, *Chem. Commun.*, 2019, **55**, 14035–14038.
64 Y. Lai, A. Halder, J. Kim, T. J. Hicks and P. J. Milner, *Angew. Chem., Int. Ed.*, 2023, **62**, e202310246.
65 A. A. Folgueiras-Amador, A. E. Teuten, M. Salam-Perez, J. E. Pearce, G. Denuault, D. Pletcher, P. J. Parsons, D. C. Harrowven and R. C. D. Brown, *Angew. Chem., Int. Ed.*, 2022, **61**, e202203694.
66 K. Mondal, S. Mallik, S. Sardana and M. Baidya, *Org. Lett.*, 2023, **25**, 1689–1694.
67 Y. Kwon, J. Lee, Y. Noh, D. Kim, Y. Lee, C. Yu, J. C. Roldao, S. Feng, J. Gierschner, R. Wannemacher and M. S. Kwon, *Nature Commun.*, 2023, **14**, 92.
68 A. F. Chmiel, O. P. Williams, C. P. Chernowsky, C. S. Yeung and Z. K. Wickens, *J. Am. Chem. Soc.*, 2021, **143**, 10882–10889.
69 Z. Li, W. Yan, X. Zhou, C. Yang, L. Guo and W. Xia, *Org. Chem. Front.*, 2025, **12**, 4946–4955.
70 L. W. Souza, N. D. Ricke, B. C. Chaffin, M. E. Fortunato, S. Jiang, C. Soylu, T. C. Caya, S. H. Lau, K. A. Wieser, A. G. Doyle and K. L. Tan, *J. Am. Chem. Soc.*, 2025, **147**, 18747–18759.
71 Kessil Lighting Ltd, *Website. Kessil LED lamps Series PR160L specification for Kessil-PR160L-440nm*, https://kessil.com/products/science_PR160L.php.
72 K. Grudzień, A. Zlobin, J. Zadworny, K. Rybicka-Jasińska and B. Sadowski, *Org. Chem. Front.*, 2024, **11**, 5232–5277.
73 M. Yan, Y. Kawamata and P. S. Baran, *Chem. Rev.*, 2017, **117**, 13230–13319.
74 S. R. Waldvogel, S. Lips, M. Selt, B. Riehl and C. J. Kampf, *Chem. Rev.*, 2018, **118**, 6706–6765.
75 X.-Q. Zhou, P.-B. Chen, Q. Xia, T.-K. Xiong, X.-J. Li, Y.-M. Pan, M.-X. He and Y. Liang, *Org. Chem. Front.*, 2023, **10**, 2039–2044.
76 N. Kurono, E. Honda, F. Komatsu, K. Orito and M. Tokuda, *Tetrahedron*, 2004, **60**, 1791–1801.
77 W. H. Koppenol and J. D. Rush, *J. Phys. Chem.*, 1987, **91**, 4429–4430.
78 Q. Shen, K. Cao, X. Wen and J. Li, *Adv. Synth. Catal.*, 2024, **366**, 4274–4293.
79 V. K. Simhadri, R. Sur and V. R. Yatham, *Eur. J. Org Chem.*, 2024, **27**, e202400490.
80 C. M. Hendy, G. C. Smith, Z. Xu, T. Lian and N. T. Jui, *J. Am. Chem. Soc.*, 2021, **143**, 8987–8992.
81 M. C. Maust, C. M. Hendy, N. T. Jui and S. B. Blakey, *J. Am. Chem. Soc.*, 2022, **144**, 3776–3781.
82 L. Zeng, J. Wang, D. Wang, H. Yi and A. Lei, *Angew. Chem., Int. Ed.*, 2023, **62**, e202309620.
83 A. Bisoyi, A. Behera, A. R. Tripathy, V. K. Simhadri and V. R. Yatham, *J. Org. Chem.*, 2024, **89**, 17818–17823.
84 Z.-Y. Ma, L.-N. Guo, Y. You, F. Yang, M. Hu and X.-H. Duan, *Org. Lett.*, 2019, **21**, 5500–5504.
85 A. L. G. Kanegusuku, T. Castanheiro, S. K. Ayer and J. L. Roizen, *Org. Lett.*, 2019, **21**, 6089–6095.
86 M. A. Short, J. M. Blackburn and J. L. Roizen, *Synlett*, 2020, **31**, 102–116.
87 M. A. Short, M. F. Shehata, M. A. Sanders and J. L. Roizen, *Chem. Sci.*, 2020, **11**, 217–223.
88 P. L. Gkizis, I. Triandafillidi and C. G. Kokotos, *Chem*, 2023, **9**, 3401–3414.
89 J. K. Mitchell, W. A. Hussain, A. H. Bansode, R. M. O'Connor, D. E. Wise, M. H. Choe and M. Parasram, *Org. Lett.*, 2023, **25**, 6517–6521.
90 D. E. Wise, E. S. Gogarnoiu, A. D. Duke, J. M. Paolillo, T. L. Vacala, W. A. Hussain and M. Parasram, *J. Am. Chem. Soc.*, 2022, **144**, 15437–15442.
91 A. Ruffoni, C. Hampton, M. Simonetti and D. Leonori, *Nature*, 2022, **610**, 81–86.
92 K. Sun, Q.-Y. Lv, Y.-W. Lin, B. Yu and W.-M. He, *Org. Chem. Front.*, 2021, **8**, 445–465.
93 C. Pratley, S. Fenner and J. A. Murphy, *Chem. Rev.*, 2022, **122**, 8181–8260.
94 H. Zhang, C. Huang, X.-A. Yuan and S. Yu, *J. Am. Chem. Soc.*, 2022, **144**, 10958–10967.
95 M. Faizan, R. Kumar, A. Mazumder, Salahuddin, N. Kukreti, A. Kumar and M. V. N. L. Chaitanya, *Chem. Biol. Drug Discov.*, 2024, **103**, e14537.
96 R. R. Kumar, B. Sahu, S. Pathania, P. K. Singh, M. J. Akhtar and B. Kumar, *ChemMedChem*, 2021, **16**, 1878–1901.
97 A. F. Brito, L. K. S. Moreira, R. Menegatti and E. A. Costa, *Fund. Clin. Pharm.*, 2019, **33**, 13–24.
98 S. Singh, R. Kumar, S. Tripathi, Salahuddin, A. Mazumder and N. Singh, *Chem. Biol. Drug Discov.*, 2025, **105**, e70077.
99 R. B. Clark and D. Elbaum, *Tetrahedron*, 2007, **63**, 3057–3065.
100 *Patent WO2003082877A1*, 2003.
101 *Patent WO2005026177A1*, 2005.
102 *US20050203296A1*, 2005.
103 B. Ma, M. Ma, T. Zhang, D. Chen and J. Yang, *J. Org. Chem.*, 2025, **90**, 13643–13656.
104 F. Dénès, M. Pichowicz, G. Povie and P. Renaud, *Chem. Rev.*, 2014, **114**, 2587–2693.
105 W. Xiao, J. Zhang and J. Wu, *ACS Catal.*, 2023, **13**, 15991–16011.
106 Y. Dang, J. Han, A. F. Chmiel, S. N. Alektiar, M. Mikhael, I. A. Guzei, C. S. Yeung and Z. K. Wickens, *J. Am. Chem. Soc.*, 2024, **146**, 35035–35042.

107 Y. Yuan, J.-C. Qi, D.-X. Wang, Z. Chen, H. Wan, J.-Y. Zhu, H. Yi, A. D. Chowdhury and A. Lei, *CCS Chem.*, 2022, **4**, 2674–2685.
108 Y. Yuan, Y. Chen, S. Tang, Z. Huang and A. Lei, *Sci. Adv.*, 2018, **4**, eaat5312.
109 C. Liu, K. Li and R. Shang, *ACS Catal.*, 2022, **12**, 4103–4109.
110 G. Laudadio, N. J. W. Straathof, M. D. Lanting, B. Knoops, V. Hessel and T. Noël, *Green Chem.*, 2017, **19**, 4061–4066.
111 T. Neveselý, M. Wienhold, J. J. Molloy and R. Gilmour, *Chem. Rev.*, 2022, **122**, 2650–2694.
112 F. Strieth-Kalthoff and F. Glorius, *Chem*, 2020, **6**, 1888–1903.